RNA-binding protein PSPC1 promotes the differentiation-dependent nuclear export of adipocyte RNAs

Jiexin Wang, Prashant Rajbhandari, Andrey Damianov, Areum Han, Tamer Sallam, Hironori Waki, Claudio J. Villanueva, Stephen D. Lee, Ronni Nielsen, Susanne Mandrup, Karen Reue, Stephen G. Young, Julian Whitelegge, Enrique Saez, Douglas L. Black, Peter Tontonoz

Research Article   Metabolism

A highly orchestrated gene expression program establishes the properties that define mature adipocytes, but the contribution of posttranscriptional factors to the adipocyte phenotype is poorly understood. Here we have shown that the RNA-binding protein PSPC1, a component of the paraspeckle complex, promotes adipogenesis in vitro and is important for mature adipocyte function in vivo. Cross-linking and immunoprecipitation followed by RNA sequencing revealed that PSPC1 binds to intronic and 3′-untranslated regions of a number of adipocyte RNAs, including the RNA encoding the transcriptional regulator EBF1. Purification of the paraspeckle complex from adipocytes further showed that PSPC1 associates with the RNA export factor DDX3X in a differentiation-dependent manner. Remarkably, PSPC1 relocates from the nucleus to the cytoplasm during differentiation, coinciding with enhanced export of adipogenic RNAs. Mice lacking PSPC1 in fat displayed reduced lipid storage and adipose tissue mass and were resistant to diet-induced obesity and insulin resistance due to a compensatory increase in energy expenditure. These findings highlight a role for PSPC1-dependent RNA maturation in the posttranscriptional control of adipose development and function.

Find the latest version:

https://jci.me/89484/pdf

RNA-binding protein PSPC1 promotes the differentiation-dependent nuclear export of adipocyte RNAs

Jiexin Wang,[1] Prashant Rajbhandari,[1] Andrey Damianov,[2] Areum Han,[2] Tamer Sallam,[3] Hironori Waki,[1] Claudio J. Villanueva,[1] Stephen D. Lee,[1] Ronni Nielsen,[4] Susanne Mandrup,[4] Karen Reue,[5] Stephen G. Young,[4,5] Julian Whitelegge,[6] Enrique Saez,[7] Douglas L. Black,[3] and Peter Tontonoz[1,8]

[1]Department of Pathology and Laboratory Medicine, Howard Hughes Medical Institute, [2]Department of Microbiology, Immunology and Molecular Genetics, and [3]Department of Medicine, UCLA, Los Angeles, California, USA. [4]Department of Biochemistry and Molecular Biology, University of Southern Denmark, Campusvej, Denmark. [5]Department of Human Genetics and [6]Pasarow Mass Spectrometry Laboratory, Semel Institute for Neuroscience and Human Behavior, UCLA, Los Angeles, California, USA. [7]Department of Chemical Physiology and The Skaggs Institute for Chemical Biology, The Scripps Research Institute, La Jolla, California, USA. [8]Molecular Biology Institute, UCLA, Los Angeles, California, USA.

A highly orchestrated gene expression program establishes the properties that define mature adipocytes, but the contribution of posttranscriptional factors to the adipocyte phenotype is poorly understood. Here we have shown that the RNA-binding protein PSPC1, a component of the paraspeckle complex, promotes adipogenesis in vitro and is important for mature adipocyte function in vivo. Cross-linking and immunoprecipitation followed by RNA sequencing revealed that PSPC1 binds to intronic and 3'-untranslated regions of a number of adipocyte RNAs, including the RNA encoding the transcriptional regulator EBF1. Purification of the paraspeckle complex from adipocytes further showed that PSPC1 associates with the RNA export factor DDX3X in a differentiation-dependent manner. Remarkably, PSPC1 relocates from the nucleus to the cytoplasm during differentiation, coinciding with enhanced export of adipogenic RNAs. Mice lacking PSPC1 in fat displayed reduced lipid storage and adipose tissue mass and were resistant to diet-induced obesity and insulin resistance due to a compensatory increase in energy expenditure. These findings highlight a role for PSPC1-dependent RNA maturation in the posttranscriptional control of adipose development and function.

Introduction

During adipogenesis, the unique structural, biochemical, and endocrine properties that define mature adipocytes are established through a complex and highly orchestrated gene expression program. Chronological expression of adipose-specific genes is achieved by sequential activation of a network of regulatory factors. To date, numerous factors have been identified that participate in the positive or negative control of adipogenesis. The vast majority of these factors are involved in transcriptional regulation (1). Peroxisome proliferator–activated receptor γ (PPARγ) is the master transcriptional regulator of adipocyte differentiation and is necessary and sufficient for the development of adipocytes (2, 3). Many genes in mature adipocytes are direct transcriptional targets of PPARγ (4–6). Other important proadipogenic transcription factors include members of the CCAAT/enhancer-binding protein (C/EBP) family, the Krüppel-like factor (KLF) family, and early B cell factors 1 and 2 (EBF1 and EBF2) (7–9). A number of factors that negatively regulate adipogenesis have also been identified, including the Wnt pathway, GATA factors, and preadipocyte factor 1 (PREF-1) (10–12). Transcriptional cofactors, such as PPARγ coactivator-1α (PGC1α), PR domain–containing 16 (PRDM16),

and transducin-like enhancer of split 3 (TLE3), have been found to interact with key transcription factors, fine-tune the adipogenic program, and/or specify white versus brown adipocyte fate (13–15).

The contribution of posttranscriptional factors to the establishment of the adipocyte phenotype is less well understood. Several microRNAs have been reported to positively or negatively affect the abundance of adipogenic RNAs through a posttranscriptional mechanism, including miR-27 and let-7 (16, 17). The pre-mRNA splicing regulator SAM68 was found to inhibit adipogenesis by controlling mTOR alternative splicing (18). Recently, the long noncoding RNA termed brown fat lncRNA 1 (BLNC1) was reported to indirectly influence the transcriptional activity of EBF2 (19). Nevertheless, in contrast with the well-established transcriptional cascade of adipogenesis, the mechanisms involved in orchestration of adipocyte development on the posttranscriptional level have been largely unexplored.

Paraspeckles are subnuclear bodies located in the interchromatin space. These protein-RNA complexes are composed of the long noncoding RNA nuclear paraspeckle assembly transport 1 (NEAT1) and 3 core protein components from the *Drosophila* behavior/human splicing (DBHS) family: paraspeckle component 1 (PSPC1), non–POU domain–containing octamer-binding protein (NONO), and splicing factor proline- and glutamine-rich (SFPQ) (20). Before the identification of paraspeckles, NONO and SFPQ were implicated in various aspects of RNA production and processing (21–25). Comparatively little is known about the cellular
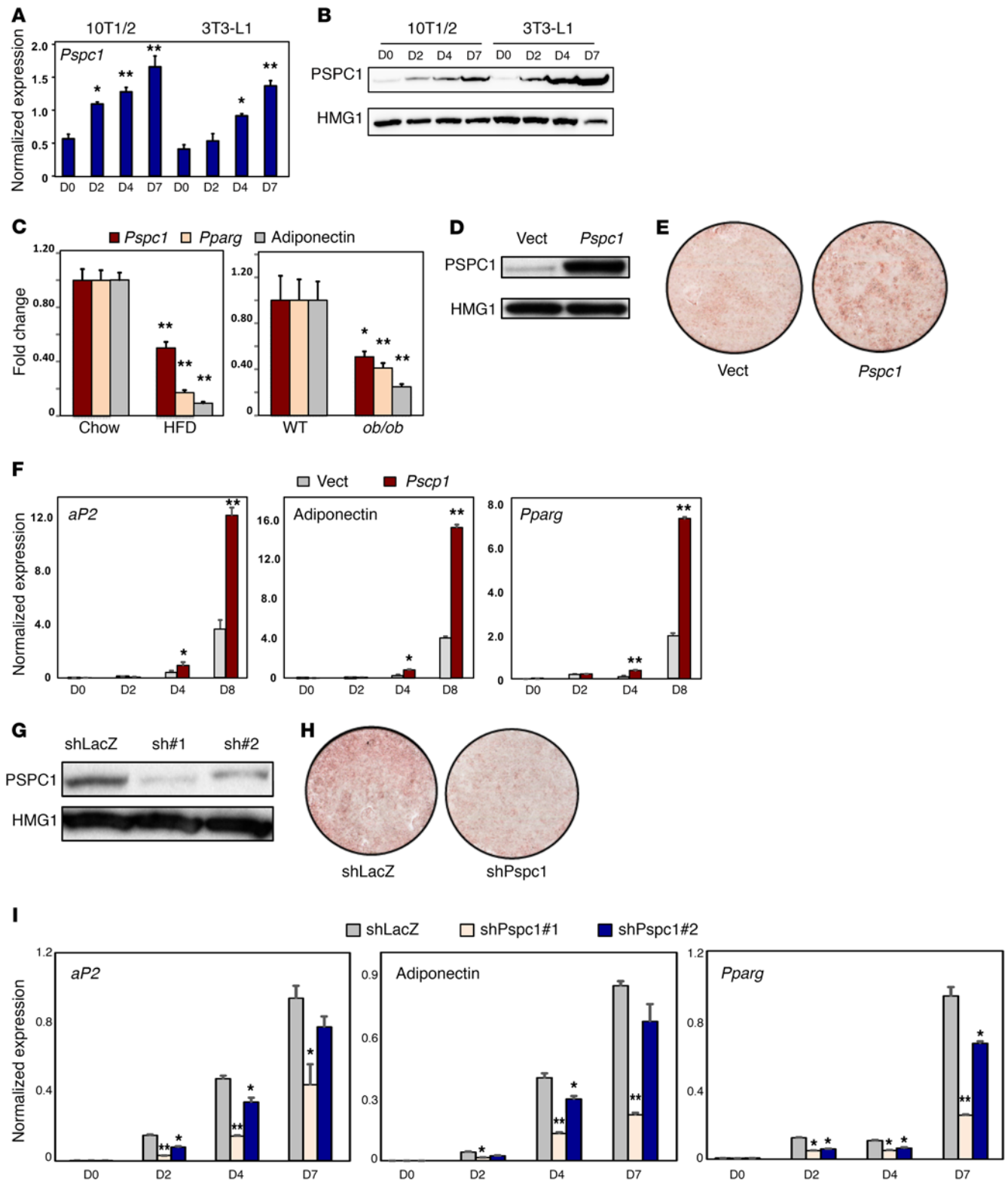
Figure 1. PSPC1 expression promotes adipogenesis. (**A**) Real-time PCR analysis of *Pspc1* mRNA during the differentiation of 10T1/2 and 3T3-L1 preadipocytes. Cells were stimulated to differentiate with dexamethasone (1 μM), IBMX (0.5 mM), insulin (5 μg/ml), and GW1929 (20 nM) for 2 days followed by insulin and GW1929 for 5 days. Comparison was made against D0 by 1-way ANOVA. Results represent 4 independent experiments. Unless mentioned otherwise, mRNA expression in this and all subsequent figures was normalized to *36B4* control. (**B**) Immunoblot analysis of PSPC1 protein during differentiation of 10T1/2 and 3T3-L1 preadipocytes. Cells were treated as in **A**. Results are representative of 3 independent experiments. (**C**) Real-time PCR analysis of *Pspc1*, *Pparg*, and adiponectin mRNA in epididymal white adipose tissue from control *ob/ob* mice and WT C57BL/6 mice fed a high-fat diet (HFD) for 12 weeks. *n* = 8–10 per group. Statistical analysis was performed using Student's *t* test. (**D**) Immunoblot analysis of PSPC1 protein expression in retrovirally derived 10T1/2 stable cell lines expressing vector or PSPC1. (**E**) Oil Red O staining of 10T1/2 stable cells described in **D**. Cells were stimulated to differentiate with DMI + 20 nM GW for 8 days. (**F**) Real-time PCR analysis of adipogenic gene expression in 10T1/2 stable cells described in **D** on different days during differentiation. Cells were stimulated to differentiate as in **E**. Comparison was made against vector control by Student's *t* test. Results represent 3 independent experiments. (**G**) Immunoblot analysis of PSPC1 protein expression in retrovirally derived 10T1/2 stable cell lines expressing PSPC1 shRNAs (shPspc1, sh#1, and sh#2) or *lacZ* shRNA (shLacZ) control. (**H**) Oil Red O staining of the 10T1/2 stable cells described in **G**. Cells were stimulated to differentiate with DMI + 20 nM GW for 7 days. (**I**) Real-time PCR analysis of adipogenic gene expression in 10T1/2 stable cells described in **G** on different days during differentiation. Cells were stimulated to differentiate as in **H**. Comparison was made against shLacZ control by 1-way ANOVA. Results are representative of 3 independent experiments. Error bars represent mean + SEM. *$P < 0.05$, **$P < 0.01$.

functions of PSPC1, although it has been suggested to be important for spermatogenesis (26, 27). Whether and how PSPC1 may play a role in RNA processing is unknown.

In the present study, we identify PSPC1 as an adipogenic factor through a phenotype-based high-throughput cDNA screen (14, 28). We further show that PSPC1 is a bona fide RNA-binding protein that shuttles from the nucleus to the cytoplasm during adipocyte differentiation. PSPC1 directly interacts with adipocyte RNAs and promotes their export, ultimately leading to increased protein expression. Loss of PSPC1 compromises adipogenesis and adipocyte gene expression both in vitro and in vivo, and affects the development of diet-induced obesity and insulin resistance. These studies shed light on the importance of PSPC1-dependent RNA maturation in adipogenesis and expand our knowledge of posttranscriptional processes contributing to adipocyte development and adipose function.

Results

PSPC1 is a direct target of PPARγ and is induced during adipogenesis. We previously performed a high-throughput screen for cDNAs affecting adipocyte differentiation (28). This screen identified TLE3 as a transcriptional modulator of adipogenic gene expression (14, 29). Another "hit" in this screen was the cDNA encoding the paraspeckle component PSPC1, which had not been previously linked with adipogenesis. To begin to address a potential function for PSPC1 in adipocytes, we first examined PSPC1 expression during the differentiation time course of 10T1/2 and 3T3-L1 preadipocytes. *Pspc1* mRNA expression rose during differentiation in both cell lines (Figure 1A), and PSPC1 protein expression was even more prominently increased (Figure 1B).

We next examined whether the *Pspc1* gene was a direct target of PPARγ. To address whether PPARγ bound directly to the *Pspc1* promoter, we analyzed genome-wide ChIP sequencing data from 3T3-L1 cells (30). We identified peaks for PPARγ and its heterodimeric partner RXRα –0.2 kb from the transcription start site in the *Pspc1* promoter (Supplemental Figure 1A; supplemental material available online with this article; doi:10.1172/JCI89484DS1), and sequence analysis identified a DR-1 sequence associated with this region (AGGTCAAGGGTTA). Directed ChIP–quantitative PCR assays confirmed that this –0.2-kb region was bound by PPARγ in a differentiation-dependent manner in 3T3-L1 cells (Supplemental Figure 1B).

PSPC1 has previously been reported to form a complex with other paraspeckle components (31). We therefore tested whether the expression of other paraspeckle components was altered during differentiation. *Sfpq* and *Nono* were modestly induced during differentiation in at least 1 cell line, and expression of *Neat1* was markedly increased in both (Supplemental Figure 1C), in agreement with a recent report (32). We also investigated whether PSPC1 level was altered in obesity. We found that *ob/ob* mice expressed less *Pspc1* mRNA in white adipose tissue (WAT) compared with WT controls (Figure 1C). We also observed reduced expression of *Pspc1* in WAT from mice fed a high-fat diet (Figure 1C and Supplemental Figure 1D). Interestingly, the expression pattern of PSPC1 in these models resembled that of PPARγ and adiponectin (Figure 1C). Examination of *Pspc1* mRNA tissue distribution revealed prominent expression in metabolically active tissues including WAT and brown adipose tissue (BAT) (Supplemental Figure 1E).

PSPC1 promotes adipogenesis in vitro. To elucidate the role of PSPC1 in adipogenesis, we overexpressed PSPC1 in 10T1/2 preadipocytes via retroviral transduction (Figure 1D and ref. 3). We obtained stable cell lines derived from large populations of clones. These lines were then induced to differentiate for 7–8 days with the with the 1 μM dexamethasone, 0.5 mM IBMX, and 5 μg/ml insulin (DMI) plus 20 nM GW1929 (GW) cocktail. Expression of PSPC1 increased the capacity of 10T1/2 cells to differentiate, as judged by Oil Red O staining (Figure 1E). Real-time PCR analysis during the differentiation time course confirmed increased expression of adipocyte-selective genes in cells overexpressing PSPC1 (Figure 1F and Supplemental Figure 1F). Comparable results were obtained in 3T3-L1 cells (Supplemental Figure 2, A and B).

As a complement to these gain-of-function studies, we expressed PSPC1 and PPARγ in combination (Supplemental Figure 2C). NIH-3T3 fibroblasts lack endogenous PPARγ expression and are therefore unable to differentiate into adipocytes. Consistent with earlier work, introduction of PPARγ conferred the ability to differentiate, as shown by the induction of adipocyte genes (3). Expression of PSPC1 alone had little, if any, effect, whereas coexpression of PSPC1 and PPARγ resulted in a synergistic effect.

In order to assess the requirement for endogenous PSPC1 expression during adipocyte differentiation, we generated retroviruses encoding shRNA sequences against *Pspc1*. Knockdown of *Pspc1* expression in 10T1/2 stable cell lines was confirmed by immunoblotting (Figure 1G). Morphological differentiation, as assessed by Oil Red O staining, was impaired in cells with reduced PSPC1 expression (Figure 1H). Reduced expression of PSPC1 was
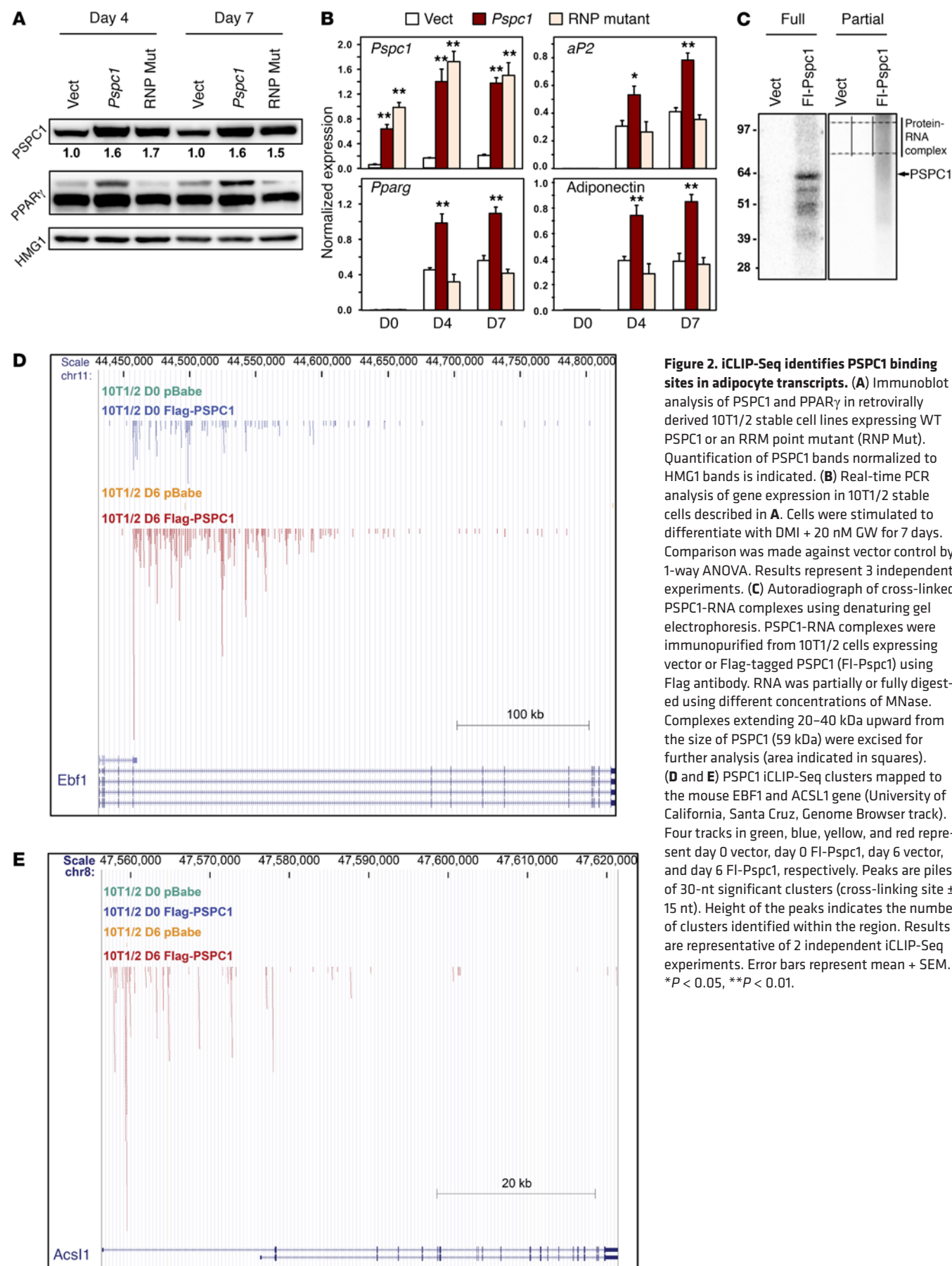
Figure 2. iCLIP-Seq identifies PSPC1 binding sites in adipocyte transcripts. (**A**) Immunoblot analysis of PSPC1 and PPARγ in retrovirally derived 10T1/2 stable cell lines expressing WT PSPC1 or an RRM point mutant (RNP Mut). Quantification of PSPC1 bands normalized to HMG1 bands is indicated. (**B**) Real-time PCR analysis of gene expression in 10T1/2 stable cells described in **A**. Cells were stimulated to differentiate with DMI + 20 nM GW for 7 days. Comparison was made against vector control by 1-way ANOVA. Results represent 3 independent experiments. (**C**) Autoradiograph of cross-linked PSPC1-RNA complexes using denaturing gel electrophoresis. PSPC1-RNA complexes were immunopurified from 10T1/2 cells expressing vector or Flag-tagged PSPC1 (Fl-Pspc1) using Flag antibody. RNA was partially or fully digested using different concentrations of MNase. Complexes extending 20–40 kDa upward from the size of PSPC1 (59 kDa) were excised for further analysis (area indicated in squares). (**D** and **E**) PSPC1 iCLIP-Seq clusters mapped to the mouse EBF1 and ACSL1 gene (University of California, Santa Cruz, Genome Browser track). Four tracks in green, blue, yellow, and red represent day 0 vector, day 0 Fl-Pspc1, day 6 vector, and day 6 Fl-Pspc1, respectively. Peaks are piles of 30-nt significant clusters (cross-linking site ± 15 nt). Height of the peaks indicates the number of clusters identified within the region. Results are representative of 2 independent iCLIP-Seq experiments. Error bars represent mean + SEM. *$P < 0.05$, **$P < 0.01$.

also associated with reduced expression of adipocyte genes (Figure 1I). Importantly, 2 different shRNA sequences targeting PSPC1 impaired adipogenesis, and the degree of knockdown correlated with the effect on adipocyte gene expression. We observed similar effects in 3T3-L1 preadipocytes engineered to stably express these shRNA sequences (Supplemental Figure 2, D and E).

We also evaluated whether NONO and SFPQ were capable of promoting adipogenesis. While ectopic expression of PSPC1 markedly increased differentiation, expression of either NONO or SFPQ alone had no effect (Supplemental Figure 2F). This finding suggests that either the adipogenic activity of PSPC1 is paraspeckle-independent or only PSPC1 levels are limiting during preadipocyte differentiation.

The adipogenic capacity of Pspc1 depends on RNA binding. Next, we addressed the mechanism of PSPC1 action in adipogenesis. All three DBHS members, PSPC1, NONO, and SFPQ, contain 2 tandem RNA recognition motifs (RRMs) that exhibit more than 50% sequence identity (33). RRMs typically engage in sequence-specific recognition of short RNA motifs (34). We investigated whether the 2 RRMs were required for PSPC1 to drive adipogenesis. We generated stable cell lines that expressed a PSPC1 protein with point mutations within the 8–amino acid RNP consensus sequence in each of its RRM domains (RNP mutant, Figure 2A), or with deletions of either RRM1 or RRM2 (Supplemental Figure 3A). Remarkably, while PSPC1 promoted adipocyte differentiation, none of the RRM mutants promoted differentiation (Figure 2B and Supplemental Figure 3B). Although the RRM1 and RRM2 deletion mutants were expressed at slightly reduced levels compared with WT (Supplemental Figure 3A), they completely lacked adipogenic activity. Immunoblotting for PPARγ in these differentiated stable cells further confirmed an almost complete loss of PSPC1 adipogenic function when the RRMs were mutated (Figure 2A). Together these data suggest that the 2 RRMs of PSPC1 are required for its adipogenic capacity.

RRM domains bind RNA with sequence-specificity. Interestingly, prior studies have shown that the presence of a second RRM in a protein confers additional affinity and specificity for RNA recognition (34, 35). We therefore postulated that PSPC1 might drive adipogenesis through interacting with mRNA transcripts of differentiation-relevant genes. To test this idea, we used individual-nucleotide resolution cross-linking and immunoprecipitation (iCLIP) coupled with high-throughput sequencing to explore whether PSPC1 binds RNA, and if so, which species (36, 37). We used 10T1/2 stable cells expressing vector or Flag-tagged PSPC1 (Fl-Pspc1). Cells before (day 0) and after (day 6) differentiation were subjected to UV cross-linking and lysed, and then protein-RNA complexes were immunoprecipitated with Flag antibody. Purified PSPC1-bound RNAs were enzymatically fragmented and radioactively labeled. When this purified PSPC1-RNA complex was resolved by SDS-PAGE, we detected a radioactive signal at the exact molecular weight of Fl-Pspc1 with full RNA digestion, and shifted above the size of Fl-Pspc1 as a smear with partial RNA digestion (Figure 2C). Radioactive signal was undetectable in the vector control pull-down samples. These data strongly suggest that PSPC1 binds to RNA directly.

To identify genome-wide RNA targets of PSPC1, we performed high-throughput sequencing on the PSPC1-bound RNA

samples recovered from the gel. We obtained 3.6 million and 3.0 million nonredundant reads from PSPC1-bound RNA on differentiation day 0 and day 6, respectively (Supplemental Table 1). We confirmed the quality of the reads (Supplemental Figure 4A) and analyzed their length distribution (Supplemental Figure 4B). Using the TopHat mapping tool, 1,024,730 (day 0) and 894,301 (day 6) reads were uniquely aligned to the mouse (NCBI37/mm9) genome (Supplemental Table 1) (38). We next used the CLIP-Seq cluster-finding algorithm CLIPper to identify 25,743 (day 0) and 38,084 (day 6) significant clusters ($P < 0.05$) (Supplemental Table 1) (39). We further analyzed the genomic distribution of PSPC1 binding sites. The majority of the binding sites (97% on day 0 and 93% on day 6) were located within intronic regions, indicating that PSPC1 preferentially interacts with pre-mRNA in the nucleus. A minority of clusters was identified within 3′-UTRs (Supplemental Figure 4C). Interestingly, we observed a 2.5-fold increase in 3′-UTR binding on day 6, suggesting a possible shift in preference or subcellular localization of the PSPC1-RNA interaction upon differentiation (Supplemental Figure 4C). Furthermore, de novo motif search with the HOMER algorithm identified AU-rich elements, UAAUU and UAUAU, within PSPC1-bound RNA sequences (Supplemental Figure 4D) (40). These analyses (library 1) were validated by a second library set (library 2) from an independently performed iCLIP-Seq experiment, reflected by approximately 70% overlap in their target transcripts (Supplemental Figure 4E).

Pspc1 binds and regulates mRNA transcripts of adipocyte-selective genes. Next, we analyzed the target mRNAs of PSPC1 based on the CLIP-defined binding sites (Supplemental Table 2). We identified several candidate PSPC1-interacting transcripts that were previously known to play important roles in adipogenesis, including *Ebf1*, *Pparg*, *Acsl1*, and *Scd1* (Figure 2, D and E, and Supplemental Figure 5). *Neat1*, a known binding partner of PSPC1, was one of the RNAs with the highest read number, confirming the validity of the assay (Supplemental Table 2). Scanning through a 15-Mb region flanking *Ebf1* on the chromosome revealed very few PSPC1 binding peaks, suggesting that our iCLIP approach had identified sequence-specific interactions (Supplemental Figure 5A).

To further validate the PSPC1-RNA interactions revealed by the iCLIP analysis, we immunoprecipitated either Fl-Pspc1 (Figure 3, A and B) or endogenous PSPC1 (Figure 3, C and D) from 10T1/2 cells and measured transcript levels by real-time PCR. Immunoprecipitated transcript levels were normalized to levels of corresponding input RNA to control for differences in transcript abundance. These studies confirmed that both native and tagged PSPC1 interacts selectively with a panel of adipocyte RNAs identified in the iCLIP analysis. Importantly, we failed to detect robust interaction of PSPC1 with several abundantly expressed differentiation-dependent adipocyte transcripts that did not appear in our iCLIP results, including *Lxra*, *Cebpa*, *Fasn*, and adiponectin (Figure 3B).

We next addressed whether binding of adipogenic transcripts by PSPC1 had functional consequences. We hypothesized that modulating the amount of PSPC1 in the cell might affect target mRNA or protein expression. To verify whether PSPC1 promotes expression of its binding targets during differentiation, we examined RNA and protein levels of these targets in differentiated 10T1/2 adipocytes on day 7. Stable expression of untagged PSPC1
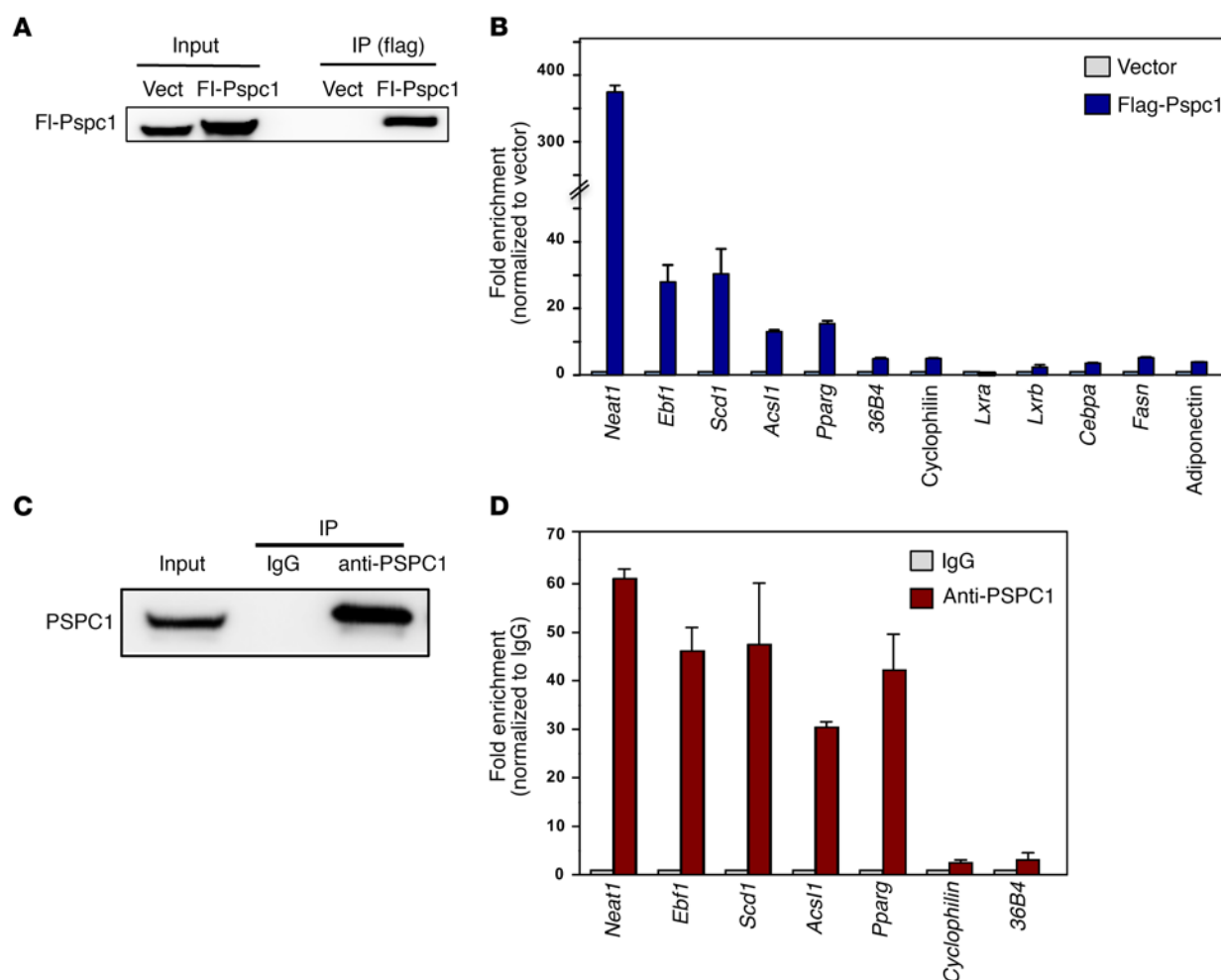
Figure 3. PSPC1 selectively interacts with certain adipocyte RNAs. (**A**) Immunoblot analysis of Flag-tagged PSPC1 protein (Fl-Pspc1) in the whole cell lysate and immunopurified products. Differentiated 10T1/2 adipocytes stably expressing Fl-Pspc1 or vector were used. Following UV cross-linking, 3X Flag antibody was used for IP. (**B**) Real-time PCR analysis of target transcript levels in Flag-immunoprecipitated samples. RNA was isolated from input and IP samples described in **A**. Values represent the amount of each transcript in the IP sample normalized to its amount in the input sample. *Neat1* serves as a positive control; cyclophilin and *36B4* serve as negative controls. Results are representative of 2 independent experiments. (**C**) Immunoblot analysis of endogenous PSPC1 protein in the whole cell lysate and immunopurified products. 10T1/2 adipocytes on differentiation day 6 were used. Following UV cross-linking, endogenous PSPC1 antibody and IgG isotype control antibody were used for IP. (**D**) Real-time PCR analysis of target transcript levels in the PSPC1-immunoprecipitated sample. RNA was isolated from input and IP samples described in **C**. Values represent the amount of each transcript in the IP sample normalized to its amount in the input sample. *Neat1* serves as a positive control; cyclophilin and *36B4* serve as negative controls. Results are representative of 2 independent experiments. Error bars represent mean + SEM.

(Psp), N-terminal Flag-tagged PSPC1 (Fl-Pspc1), or C-terminal Flag-tagged PSPC1 (Pspc1-Fl) all conferred increased levels of target mRNAs and proteins (Figure 4, A and B, and Supplemental Figure 6A). By contrast, point mutations in the 2 RRM domains abolished the effects. Furthermore, stable expression of native PSPC1 but not the RRM deletion mutants resulted in elevated expression levels of both target proteins and mRNAs on day 6 (Supplemental Figure 6, B and C).

To discriminate between direct and indirect — or between transcriptional and posttranscriptional — effects, we assessed the effects of PSPC1 in undifferentiated 10T1/2 preadipocytes to eliminate secondary effects due to differentiation. Remarkably, while native PSPC1 expression did not affect target mRNA levels (Figure 4C), target protein levels were increased (Figure 4D and Supplemental Figure 6D), suggesting a posttranscriptional

mechanism. This effect was not observed with the RRM deletion mutants. Although the RRM deletion mutants were expressed at slightly reduced levels compared with WT, they completely lacked activity, suggesting that the RRM domains are likely to contribute to these effects. Conversely, loss of endogenous PSPC1 strongly reduced protein levels of PSPC1 targets, with only minimal or no effect on mRNA expression (Figure 4, E and F, and Supplemental Figure 6E). Since these effects of PSPC1 expression and knockdown were observed in the absence of differentiation, they were likely to be primary effects of PSPC1 modulation.

Pspc1 interacts with DDX3X in a differentiation- and RNA-dependent manner. RNA-binding proteins tend to form complexes that work cooperatively on the target RNA molecule. Paraspeckle complexes have not heretofore been studied in adipocytes, and therefore their composition in this cell type is unknown.
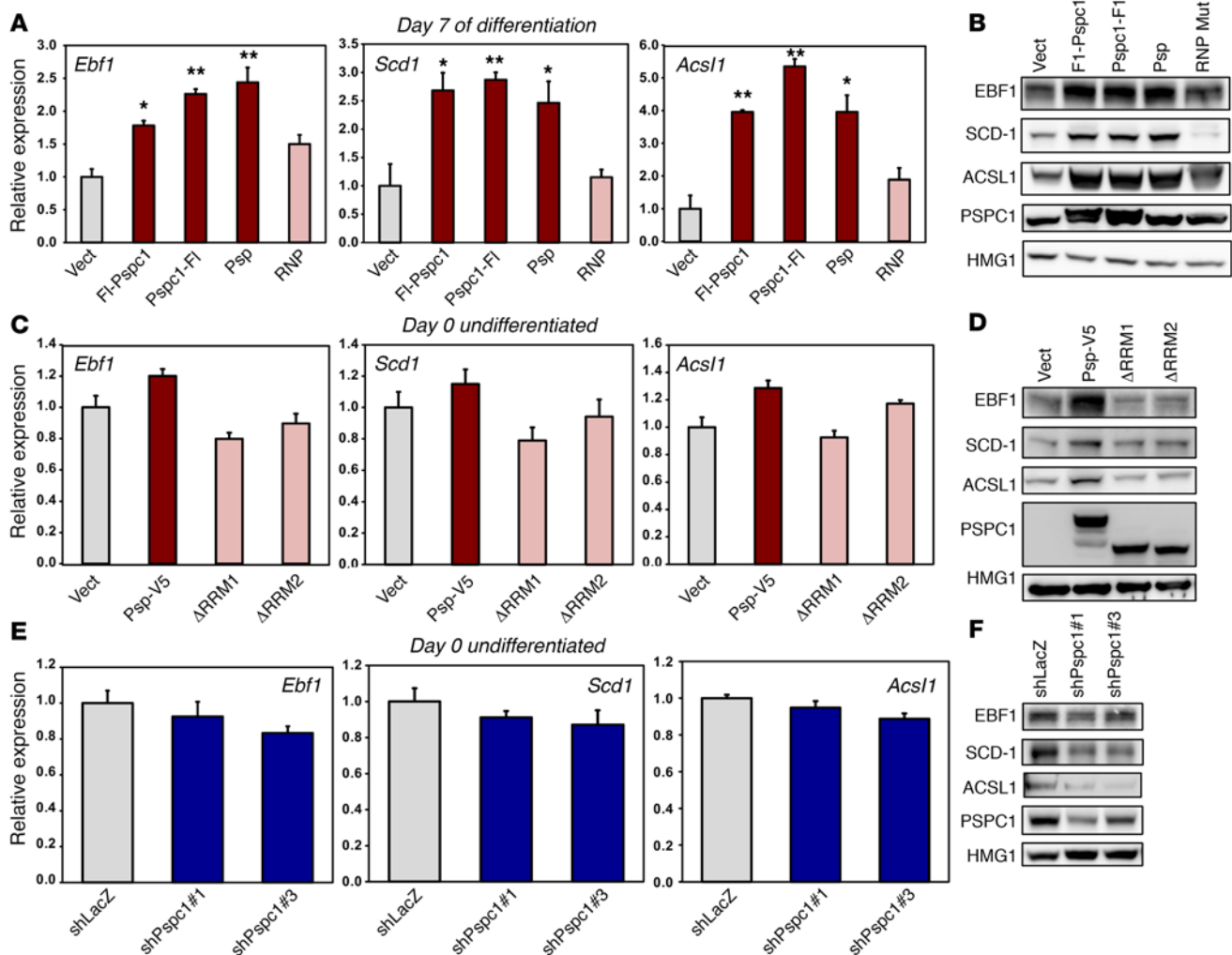
Figure 4. PSPC1 influences the expression of iCLIP-identified target RNAs. (**A**) Real-time PCR analysis of target gene mRNA expression in differentiated 10T1/2 cells stably expressing vector (Vect), N-terminal Flag-tagged PSPC1 (Fl-Pspc1), C-terminal Flag-tagged PSPC1 (Pspc1-Fl), untagged PSPC1 (Psp), or PSPC1 RNP mutant (RNP). Cells were stimulated to differentiate with DMI + 20 nM GW for 7 days. Comparison was made against vector control by 1-way ANOVA. Results represent 3 independent experiments. (**B**) Immunoblot analysis of target gene protein expression in differentiated 10T1/2 stable cell lines described in **A**. Results are representative of 3 independent experiments. (**C**) Real-time PCR analysis of target gene mRNA expression in undifferentiated 10T1/2 cells expressing vector (Vect), V5-tagged WT PSPC1 (Psp-V5), V5-tagged RRM1 deletion mutant (RRM1), or V5-tagged RRM2 deletion mutant (RRM2). Comparison was made against vector control by 1-way ANOVA. Results represent 3 independent experiments. (**D**) Immunoblot analysis of target gene protein expression in undifferentiated 10T1/2 cells described in **C**. Results are representative of 3 independent experiments. The immunoblots presented in **D** include replicate samples run on a parallel gel. (**E**) Real-time PCR analysis of target gene mRNA expression in undifferentiated 10T1/2 cells expressing PSPC1 shRNAs (shPspc1#1 and shPspc1#3) or *lacZ* shRNA control (shLacZ). Comparison was made against shlacZ control by 1-way ANOVA. Results represent 3 independent experiments. (**F**) Immunoblot analysis of target gene protein expression in undifferentiated 10T1/2 cells described in **E**. Results are representative of 3 independent experiments. Error bars represent mean + SEM. *$P < 0.05$, **$P < 0.01$.

We hypothesized that determining the PSPC1 protein interactome in adipocytes might provide insight into the mechanism by which PSPC1-RNA binding regulates gene expression. We used coimmunoprecipitation (co-IP) coupled with mass spectrometry to investigate the constituents of PSPC1 complexes in preadipocytes and adipocytes. We analyzed 10T1/2 stable cell lines that expressed Fl-Pspc1 at 2 differentiation time points (days 0 and 7). Silver staining of the immunoprecipitated proteins revealed a number of bands that were enriched in the Fl-Pspc1 sample on day 7 (Figure 5A, arrows). Mass spectrometry analysis of the immunoprecipitated proteins generated a list of putative PSPC1 binding partners. To eliminate nonspecific binding, the list of candidates was compared with the sample from cells lacking Fl-Pspc1. Impor-

tantly, the 2 known PSPC1 interaction partners, NONO and SFPQ, had the highest confidence scores, confirming the validity of our approach. Among the other top interaction candidates, the majority were known RNA-binding proteins, reinforcing the idea that PSPC1 is involved in RNA biology. Notably, the 2 categories with the highest number of interaction candidates were "RNA transport" and "protein synthesis" (Supplemental Table 3).

We verified the interaction of candidates from our list using co-IP studies (Figure 5B and data not shown). One interacting protein, DEAD-box RNA helicase 3 (DDX3X), was of particular interest. First, it ranked alongside the known direct interactors, NONO and SFPQ; second, it was associated with PSPC1 in a differentiation-dependent manner (Figure 5B). The finding that PSPC1-DDX3X asso-
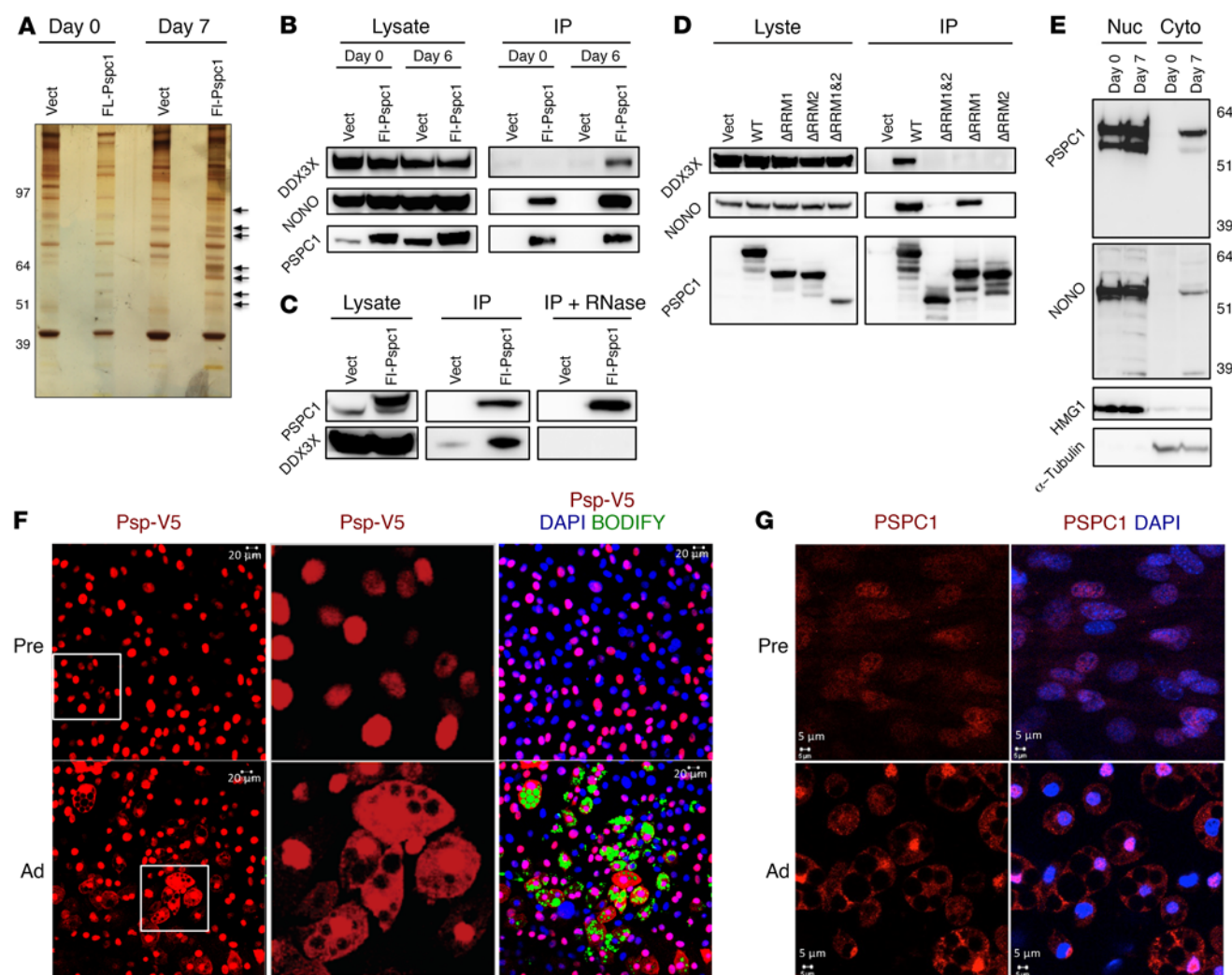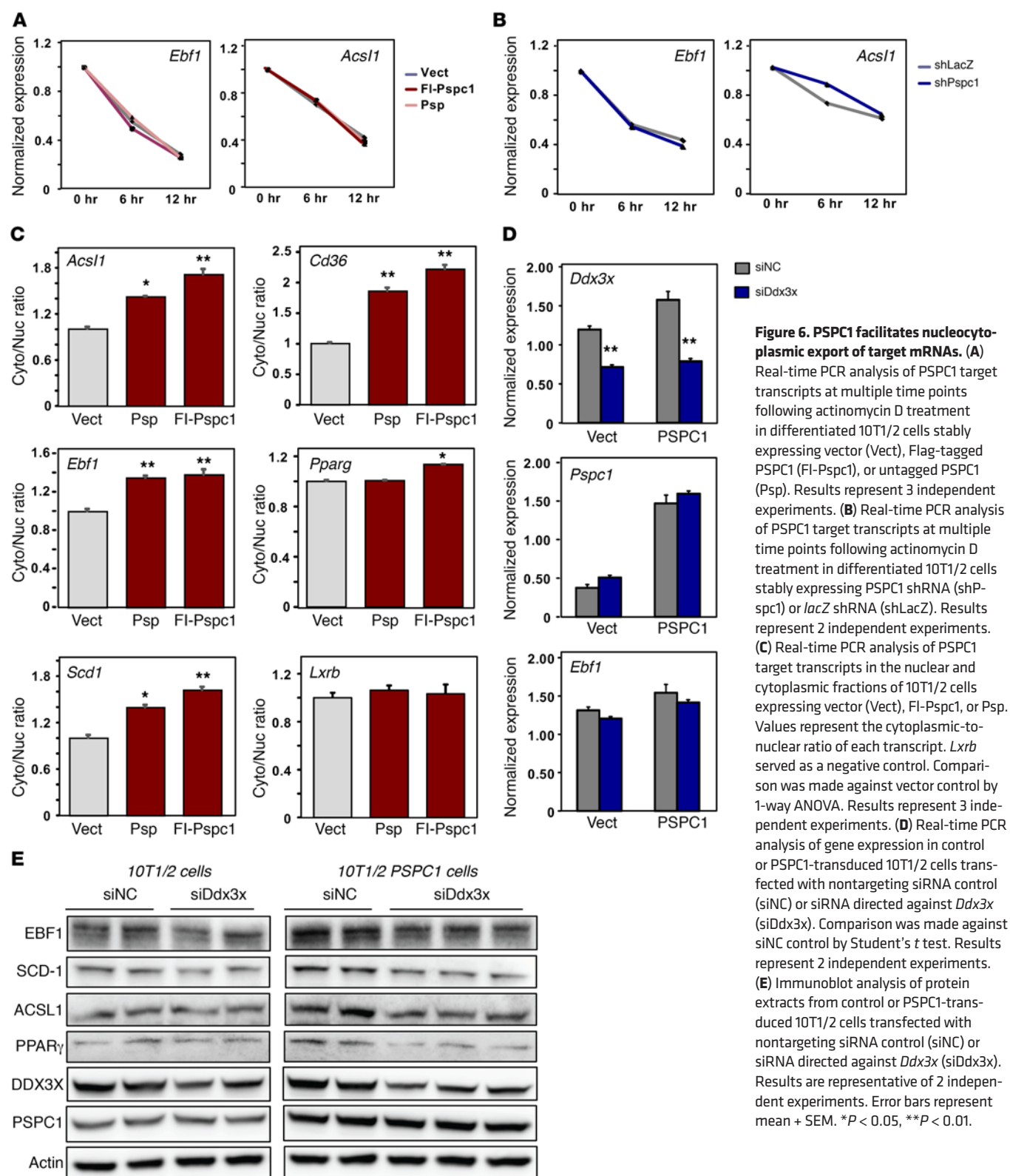
Figure 5. PSPC1 interacts with DDX3X and translocates from nucleus to cytoplasm during differentiation. (**A**) Silver staining of Flag-tagged PSPC1 (Fl-Pspc1) coimmunoprecipitated proteins on a gradient Bis-Tris gel. Co-IP with Flag antibody was performed in 10T1/2 cells stably expressing Fl-Pspc1 or vector. Arrows indicate bands present exclusively in the Fl-Pspc1 lane. (**B**) Immunoblot analysis of proteins coimmunoprecipitated with Fl-Pspc1 in 10T1/2 cells on differentiation day 0 and day 6. Cells were stimulated to differentiate with DMI + 20 nM GW. The known interaction partner NONO served as a positive control. Results are representative of 3 independent experiments. (**C**) Immunoblot analysis of DDX3X coimmunoprecipitated with Fl-Pspc1 in 10T1/2 cells on differentiation day 6 (middle panel). Cell lysates were treated with control or RNase prior to IP (right panel). Results are representative of 2 independent experiments. (**D**) Immunoblot analysis of DDX3X and NONO co-IP with PSPC1 and RRM mutants (ΔRRM1 and ΔRRM2). 10T1/2 stable cells were stimulated to differentiate with DMI + 20 nM GW. Results are representative of 2 independent experiments. (**E**) Immunoblot analysis of PSPC1 and NONO in the nuclear (Nuc) and cytoplasmic (Cyto) fractions of 10T1/2 cells on differentiation days 0 and 7. Cells were stimulated to differentiate with DMI + 20 nM GW. HMG1 and α-tubulin served as nuclear and cytoplasmic markers, respectively. Results are representative of 3 independent experiments. (**F**) PSPC1 subcellular localization visualized by fluorescent confocal microscopy in undifferentiated (Pre) and differentiated (Ad) 10T1/2 adipocytes stably expressing V5-tagged PSPC1 (Psp-V5). Cells were stimulated to differentiate with DMI + 20 nM GW for 7 days. Scale bars: 20 μm. Results are representative of 2 independent experiments. (**G**) PSPC1 subcellular localization visualized by fluorescent confocal microscopy in undifferentiated (Pre) and differentiated (Ad) 10T1/2 adipocytes stably expressing untagged PSPC1. Antibody against PSPC1 (red) was used for detecting endogenous PSPC1. Scale bars: 5 μm. Results are representative of 3 independent experiments.

ciation was induced by differentiation suggested it could have functional relevance to adipogenesis. Since both PSPC1 and DDX3X are RNA-binding proteins (41), we examined whether their interaction was RNA-dependent. Treatment with RNase prior to IP of PSPC1 abolished the PSPC1-DDX3X interaction, indicating that it was indeed RNA-dependent (Figure 5C). To determine whether the RNA-interacting RRMs were required for interaction with various PSPC1 complex components in adipocytes, we performed IPs with WT and RRM mutant PSPC1 proteins. We found that RRM2 was

selectively required for interaction of PSPC1 with NONO, while both RRMs were required for interaction with DDX3X (Figure 5D).

Pspc1 translocates from nucleus to cytoplasm upon adipocyte differentiation. DDX3X is an ATP-dependent RNA helicase that participates in various aspects of mRNA metabolism, including mRNA nuclear export (42–44). Prior studies have shown that DDX3X interacts with mRNA ribonucleoprotein complexes in the nucleus and is exported along with the ribonucleoproteins to the cytoplasm (45–47). We therefore speculated that PSPC1, in a com-

Figure 6. PSPC1 facilitates nucleocytoplasmic export of target mRNAs. (A) Real-time PCR analysis of PSPC1 target transcripts at multiple time points following actinomycin D treatment in differentiated 10T1/2 cells stably expressing vector (Vect), Flag-tagged PSPC1 (Fl-Pspc1), or untagged PSPC1 (Psp). Results represent 3 independent experiments. **(B)** Real-time PCR analysis of PSPC1 target transcripts at multiple time points following actinomycin D treatment in differentiated 10T1/2 cells stably expressing PSPC1 shRNA (shPspc1) or *lacZ* shRNA (shLacZ). Results represent 2 independent experiments. **(C)** Real-time PCR analysis of PSPC1 target transcripts in the nuclear and cytoplasmic fractions of 10T1/2 cells expressing vector (Vect), Fl-Pspc1, or Psp. Values represent the cytoplasmic-to-nuclear ratio of each transcript. *Lxrb* served as a negative control. Comparison was made against vector control by 1-way ANOVA. Results represent 3 independent experiments. **(D)** Real-time PCR analysis of gene expression in control or PSPC1-transduced 10T1/2 cells transfected with nontargeting siRNA control (siNC) or siRNA directed against *Ddx3x* (siDdx3x). Comparison was made against siNC control by Student's *t* test. Results represent 2 independent experiments. **(E)** Immunoblot analysis of protein extracts from control or PSPC1-transduced 10T1/2 cells transfected with nontargeting siRNA control (siNC) or siRNA directed against *Ddx3x* (siDdx3x). Results are representative of 2 independent experiments. Error bars represent mean + SEM. *$P < 0.05$, **$P < 0.01$.

plex with DDX3X, might be exported out of the nucleus (together with its target mRNA) during adipogenesis. To test this hypothesis, we performed nuclear-cytoplasmic fractionation on undifferentiated and differentiated adipocytes. Before differentiation (day 0), PSPC1 was present solely in the nuclear fraction. Surprisingly,

despite previous reports that PSPC1 was a constitutively nuclear protein, we detected a substantial fraction of PSPC1 protein in the cytoplasmic fraction on day 7 (Figure 5E). This finding suggested that PSPC1 might accompany its target mRNA transcripts from the nucleus into the cytoplasm during differentiation.
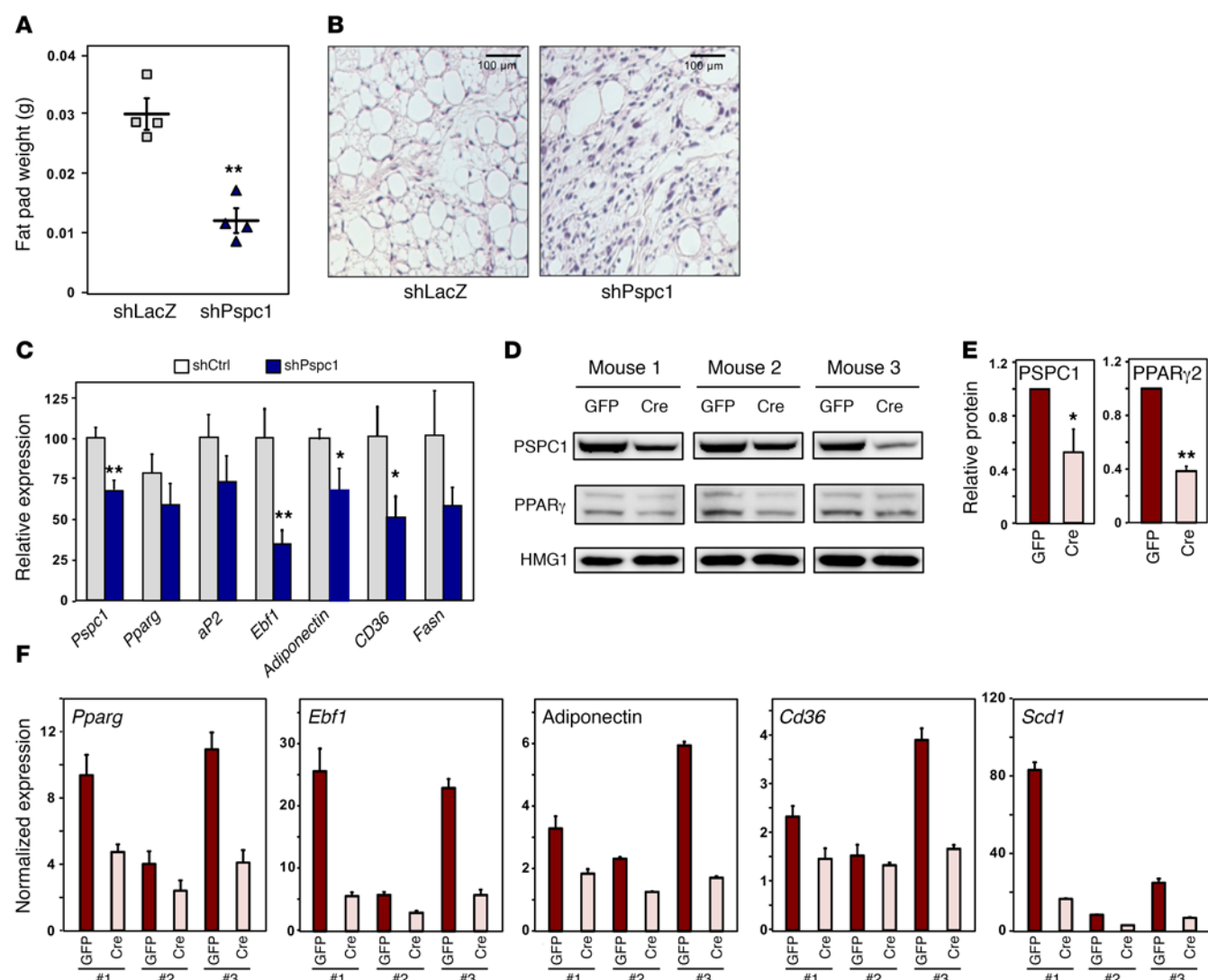
Figure 7. PSPC1 is important for adipocyte differentiation and maintenance in vivo. (**A**) Weight of the fat pad formed from subcutaneous transplantation of 3T3-F442A preadipocytes expressing *lacZ* shRNA (shLacZ) or PSPC1 shRNA (shPspc1). Mice were sacrificed 4 weeks after transplantation. Six-week old male NCr nude mice were used, *n* = 4 per group. Statistical analysis was performed using Student's *t* test. (**B**) Histological analysis of the fat pad formed from subcutaneous preadipocyte transplantation described in **A**. Scale bars: 100 μm. (**C**) Real-time PCR analysis of *Pspc1* and adipose-specific genes in the fat pads formed from the subcutaneous preadipocyte transplantations described in **A**. Comparison was made against shCtrl by Student's *t* test. (**D**) Immunoblot analysis of PSPC1 and PPARγ protein expression in the inguinal WAT of each *Pspc1^fl/fl* mouse injected with GFP adenovirus in 1 inguinal fat pad and Cre adenovirus in the contralateral pad. Mice were sacrificed 7 days after adenovirus injection. Eight-week-old male *Pspc1^fl/fl* mice were used, *n* = 5. Results from 3 representative mice are shown. (**E**) Quantification of band intensity in **D**. Values represent intensity of PSPC1 or PPARγ2 bands normalized to intensity of corresponding HMG1 bands. Means of 3 representative mice are presented. (**F**) Real-time PCR analysis of adipose-specific genes in the inguinal WAT injected with adenovirus as described in **D**. Results from 3 representative mice are shown. Results are representative of 2 independent cohorts of mice. Error bars represent mean + SEM. *$P < 0.05$, **$P < 0.01$.

To provide additional evidence for PSPC1 translocation, we used confocal immunofluorescence microscopy to visualize PSPC1 localization in preadipocytes and adipocytes. In preadipocytes, PSPC1 expression entirely colocalized with DAPI staining, consistent with nuclear localization. However, in mature adipocytes, there was a remarkable shift of PSPC1 staining into the cytoplasm, consistent with results of our cell fractionation studies (Figure 5, F and G). In particular, the lipid-laden cells displayed prominent cytoplasmic PSPC1 localization. Parallel studies were carried out with both epitope-tagged and endogenous PSPC1 protein. These data indicate that PSPC1 shuttles from the nucleus to the cytoplasm during adipocyte differentiation.

Pspc1 promotes nuclear export of adipogenic mRNAs. The discovery of PSPC1 translocation suggested that PSPC1 might facilitate adipocyte differentiation through a mechanism(s) affecting mRNA processing, transport, or stability. We initially tested whether PSPC1 enhanced target mRNA stability in the cytoplasm. We treated 10T1/2 adipocytes with actinomycin D to inhibit transcription and analyzed target transcript levels. We were unable to detect any alteration in rates of target mRNA degradation in cells with either increased or decreased PSPC1
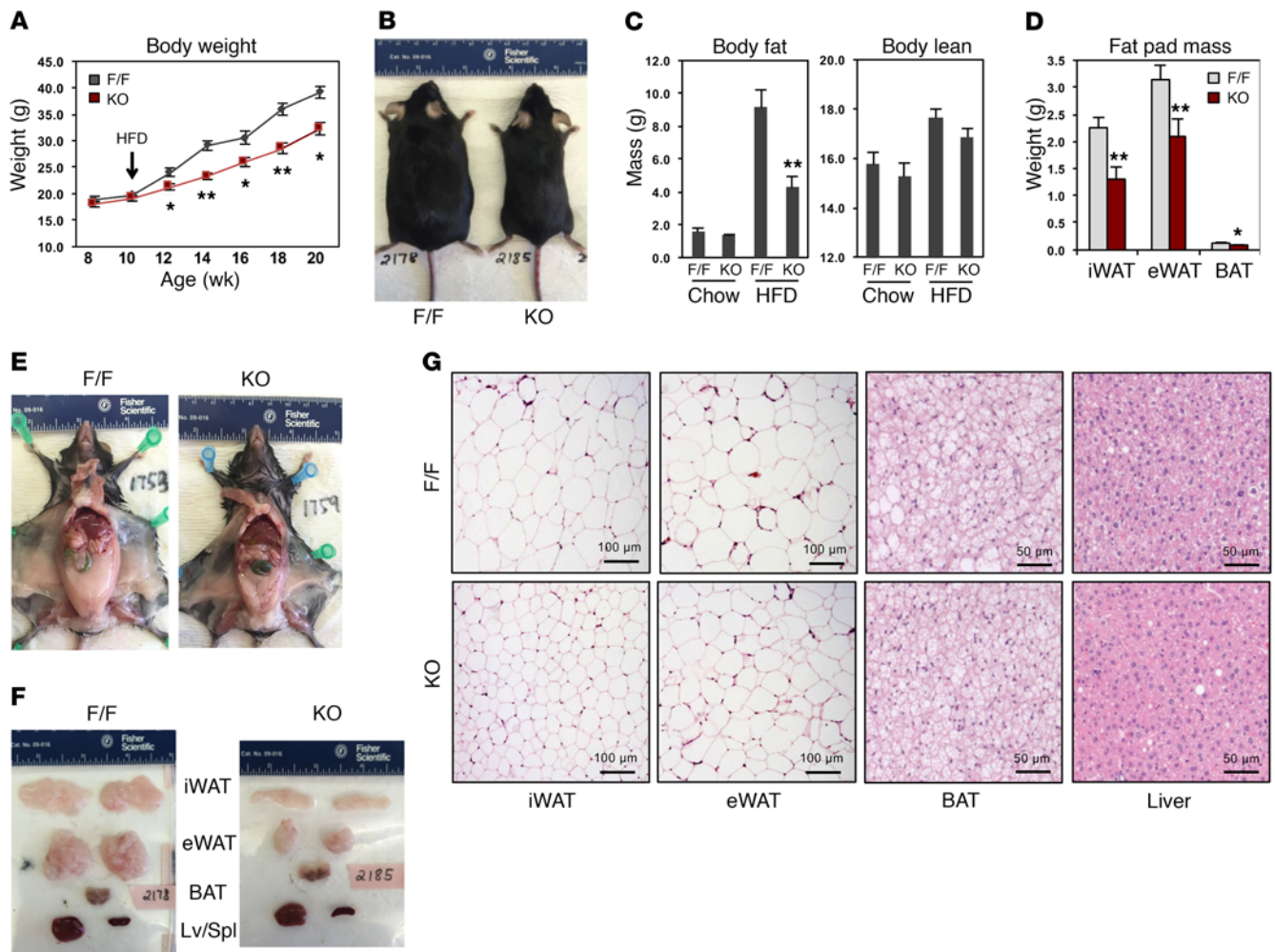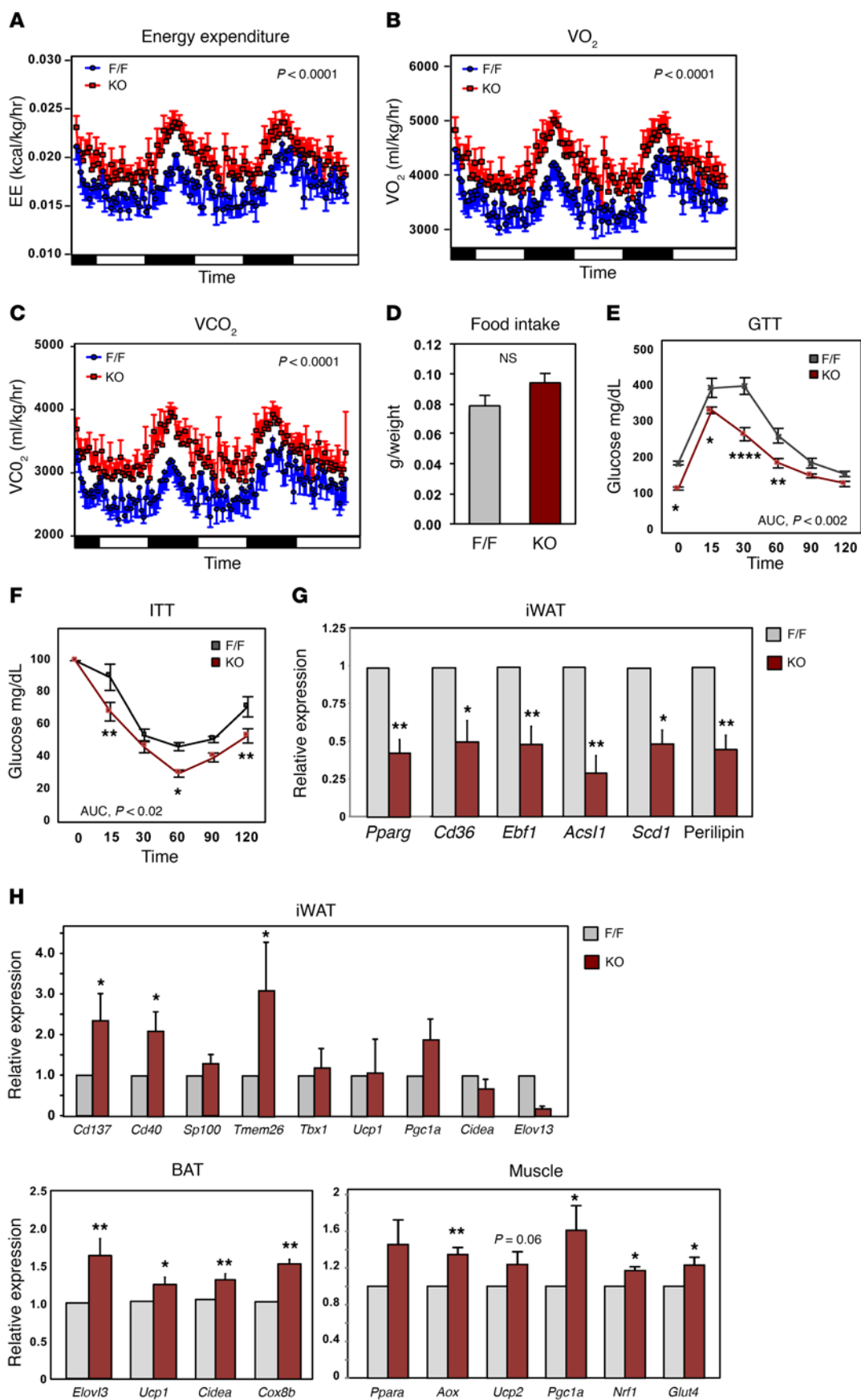
Figure 8. Adipose-specific PSPC1-deficient mice are resistant to diet-induced obesity. (**A**) Body weight of *Pspc1*^{fl/fl} (F/F) and *Pspc1*^{fl/fl} *Cre+* (KO) mice fed chow diet for 10 weeks and then switched to 60% HFD. *n* = 8 per group, female mice. Statistical analysis was performed using Student's *t* test. (**B**) External appearance of representative F/F and KO mice shown in **A** at 20 weeks of age after 10 weeks on HFD. (**C**) Body fat and lean mass in F/F and KO mice at 8 weeks old on chow diet and at 20 weeks old after 10 weeks on HFD determined by EchoMRI. *n* = 8 per group, female mice. Comparison was made against F/F control mice by Student's *t* test. (**D**) Average weight of individual white and brown adipose fat pads from F/F and KO mice after 10 weeks on HFD. *n* = 8 per group, 20-week-old female mice. Comparison was made against F/F control mice by Student's *t* test. (**E**) Representative F/F and KO mice after 10 weeks on HFD showing grossly reduced adipose tissue content in the absence of PSPC1. (**F**) Gross appearance of tissues from F/F and KO mice after 10 weeks on HFD. (**G**) Histology of tissues from F/F and KO mice after 10 weeks on HFD. Results are representative of 2 independent cohorts of mice. Scale bars: iWAT and epididymal white adipose tissue (eWAT), 100 μm; BAT and liver, 50 μm. Error bars represent mean + SEM. *$P < 0.05$, **$P < 0.01$.

(Figure 6, A and B), suggesting that PSPC1 does not stabilize these transcripts.

We next addressed whether PSPC1 was able to facilitate mRNA export from the nucleus. We performed nuclear-cytoplasmic fractionation (Supplemental Figure 7A) and analyzed PSPC1-interacting RNAs in each fraction. Adipocytes stably expressing native or Flag-tagged PSPC1 exhibited an elevated cytoplasmic-to-nuclear ratio of a number of mRNA targets compared with control cells, including *Ebf1*, *Pparg*, *Acsl1*, *Scd1*, and *Cd36* (Figure 6C). Importantly, this finding did not appear to reflect a general effect on all mRNAs, as those not found to interact with PSPC1, such as *Lxrb*, were not different between control and PSPC1-expressing cells. These observations suggest that PSPC1 facilitates adipocyte differentiation by promoting the nuclear export of a subset of mRNAs, resulting in augmented protein expression. In support of this idea,

we found that expression of the putative mRNA export factor DDX3X, with which PSPC1 interacts (Figure 5), was important for PSPC1 effects on its target protein expression. We knocked down DDX3X expression with siRNA in preadipocytes expressing retroviral vector alone or PSPC1. Even partial loss of DDX3X protein led to a reduction in protein levels of EBF1, SCD-1, ASCL1, and PPARγ, without affecting levels of their corresponding mRNAs and without affecting levels of PSPC1 protein (Figure 6, D and E, and Supplemental Figure 7, B and C). This effect was most evident in cells overexpressing PSPC1 (Figure 6E, right), consistent with the hypothesis that DDX3X facilitates the action of PSPC1.

Pspc1 is required for adipogenesis in vivo. Finally, we tested the importance of PSPC1 for adipocyte differentiation and maintenance in vivo. To address whether PSPC1 activity contributes to adipocyte development, we assessed the capacity of PSPC1

Figure 9. Adipose-specific PSPC1-deficient mice exhibit increased energy expenditure and glucose tolerance. (**A**–**C**) Energy expenditure rate (EE; kcal/kg/h), VO_2 (ml/kg/h), and VCO_2 (ml/kg/h) of $Pspc1^{fl/fl}$ (F/F) and $Pspc1^{fl/fl}$ Cre+ (KO) mice were analyzed by Columbus Oxymax metabolic chambers after 4 weeks on HFD. Twelve-hour light/dark cycles, 72-hour total duration; each light/dark bar represents 12-hour duration. n = 8 per group, female mice. Statistical analysis was performed using 2-way ANOVA. (**D**) Daily food intake normalized to body weight. n = 8 per group, female mice. Comparison was made against F/F control mice by Student's t test. (**E**) IP glucose tolerance test (GTT) performed on F/F and KO mice after 4 weeks of HFD feeding. n = 5 per group, 14-week-old female mice. Comparison at each time point was made against F/F control mice by repeated-measures ANOVA. *P < 0.05, **P < 0.01, ****P < 0.0001. (**F**) Insulin tolerance test (ITT) performed on F/F and KO mice after 10 weeks of HFD feeding. n = 5 per group, 20-week-old female mice. Comparison at each time point was made against F/F control mice by repeated-measures ANOVA. (**G**) Relative gene expression in iWAT from F/F and KO mice after 10 weeks on HFD determined by real-time PCR. n = 8 per group, 20-week-old female mice. Comparison was made against F/F control mice by Student's t test. (**H**) Relative gene expression in iWAT, BAT, and skeletal muscle from F/F and KO mice after 10 weeks on HFD determined by real-time PCR. n = 8 per group, 20-week-old female mice. Comparison was made against F/F control mice by Student's t test. Results are representative of 2 independent cohorts of mice. Error bars represent mean + SEM. *P < 0.05, **P < 0.01.

knockdown preadipocytes to form fat pads when transplanted into immunocompromised mice. We used 3T3-F442A cells for these studies, as they efficiently form fat pads (48). Four weeks after subcutaneous transplantation, preadipocytes transduced with PSPC1 shRNA (shPspc1) gave rise to markedly smaller fat pads compared with controls. The average fat pad weight was lower, suggesting that fewer adipocytes were derived from PSPC1 knockdown preadipocytes compared with controls (Figure 7A). Histological analysis of the control fat pads revealed primarily mature adipocytes with large unilocular lipid droplets, resembling WAT. By contrast, fat pads from the shPspc1 group contained more stromal tissue and relatively few adipocytes, suggesting that cells with decreased PSPC1 expression had impaired differentiation capacity in vivo (Figure 7B). Gene expression analysis also revealed lower levels of adipocyte mRNAs in the shPspc1 fat pads (Figure 7C). Comparable results were obtained for multiple shRNA constructs in multiple independent experiments (Supplemental Figure 8A).

As a complementary approach to address PSPC1 function *in vivo*, we generated *Pspc1*-floxed mice (*Pspc1^fl/fl^*) (Supplemental Figure 8, B and C) and used Cre-expressing adenovirus to delete *Pspc1* in inguinal WAT. We injected inguinal fat pads of *Pspc1^fl/fl^* mice with Ad-Cre virus on 1 side and Ad-GFP control virus on the other. All comparisons were made between the 2 fat pads within the same animal. The efficacy of adenoviral transduction was confirmed by diminished PSPC1 protein expression in the Ad-Cre–injected fat pads (Figure 7, D and E). PSPC1 expression was not altered in the nearby quadriceps muscle or in the liver (Supplemental Figure 8D). Adipocyte-specific gene expression was lower in Ad-Cre–injected fat pads compared with their Ad-GFP–injected counterparts, including a number of the CLIP-identified PSPC1 target genes (Figure 7F). The results of Figure 7 indicate that endogenous PSPC1 is indispensable for adipose tissue development and maintenance in vivo.

Resistance to diet-induced obesity in adipose-specific Pspc1 knockout mice. To address the consequence of chronic loss of PSPC1 in mature adipose tissue, we generated adipose tissue–specific *Pspc1*-null mice by crossing the floxed mice with adiponectin-*Cre* transgenics. Comparisons were made between littermate homozygous *Pspc1*-floxed mice in the presence or absence of the *Cre* transgene. As expected, mice expressing adiponectin-*Cre* showed markedly reduced *Pspc1* mRNA expression in WAT and BAT (Supplemental Figure 9A). Adipose PSPC1–deficient mice had body weight comparable to that of controls when maintained on chow diet (Figure 8A). However, when the mice were switched to a high-fat diet (60% calories from fat), they gained much less weight (Figure 8A) and were visibly leaner (Figure 8B). MRI analysis of body composition after 10 weeks on a high-fat diet confirmed reduced body fat in adipose PSPC1–deficient mice with no change in body lean mass (Figure 8C). On visual inspection after laparotomy, adipose PSPC1–deficient mice had much less adipose tissue, and the size and weight of individual fat pads were correspondingly reduced (Figure 8, D–F). The size of white adipocytes in both the inguinal white adipose tissue (iWAT) and the epididymal white adipose tissue (eWAT) depots was smaller in adipose PSPC1–deficient mice (Figure 8G). Both the BAT and the liver of adipose PSPC1–deficient mice showed histological evidence of rescued lipid accumulation compared with controls (Figure 8G). Spleen and liver size was not different between groups (Figure 8F). Plasma triglyceride and cholesterol levels were also not different (Supplemental Figure 9B).

We next asked whether adipose-specific *Pspc1* deletion might result in altered systemic energy balance. Surprisingly, metabolic cage analysis revealed a dramatic elevation in VO_2, VCO_2, and energy expenditure rate (EE) in mice lacking adipose PSPC1 compared with floxed controls (Figure 9, A–C, and Supplemental Figure 9C). Further analysis of the EE data using analysis of covariance (ANCOVA) with body mass or lean mass as covariant confirmed an increase in EE in adipose PSPC1–deficient mice compared with controls (Supplemental Figure 9D). Food intake was not different between genotypes (Figure 9D). Activity was slightly increased in adipose PSPC1–deficient mice (Supplemental Figure 9E).

We went on to explore whether loss of adipose PSPC1 expression affected systemic metabolism in the setting of a high-fat diet challenge. Mice lacking PSPC1 in adipose tissue fed with a high-fat diet had improved glucose tolerance compared with controls (Figure 9E). Furthermore, insulin tolerance tests revealed an improved response to exogenous insulin in PSPC1-deficient mice, suggesting that loss of PSPC1 expression ameliorates the development of high-fat diet–induced insulin resistance (Figure 9F).

Consistent with the finding that PSPC1 expression affects adipocyte gene expression, we found reduced expression of multiple adipocyte genes in iWAT from adipose PSPC1–deficient mice (Figure 9G). Interestingly, there was increased expression of genes linked to beiging in iWAT and increased expression of thermogenic genes in BAT in PSPC1-deficient mice compared with controls (Figure 9H). This finding is unlikely to reflect direct antagonistic actions of PSPC1 on thermogenic genes, as overexpression of PSPC1 promoted brown adipocyte differentiation in vitro (Supplemental Figure 9F). Furthermore, despite the fact that *Pspc1* deletion was specific for adipose tissue, we also found elevated expression of genes involved in fatty acid utilization, including that encoding acyl-CoA oxidase, in the skeletal muscle of adipose PSPC1–deficient mice

(Figure 9H). These data suggest that loss of PSPC1 expression in adipose tissue provokes compensatory changes in systemic energy balance that offset the impairment in adipose tissue lipid storage. In addition, GLUT4 expression levels were elevated in the skeletal muscle of adipose PSPC1–deficient mice, potentially contributing to their improved glucose tolerance (Figure 9H). Collectively, our results indicate that the ability of PSPC1 to regulate adipocyte mRNA maturation is important for both adipocyte development and the function of mature adipose tissue in vivo.

Discussion

Adipogenesis involves different levels of regulation, with the majority of known control factors exerting their effects at the transcriptional level. In the present study, we delineated a role for the RNA-binding protein PSPC1 in adipocyte differentiation. PSPC1 is a direct target of PPARγ, and its expression is induced during differentiation. Complementary in vitro and in vivo analyses demonstrated that PSPC1 expression facilitates adipocyte-specific protein expression and adipogenesis. Deletion of PSPC1 in mature fat in vivo impairs adipocyte-specific gene expression and reduces adipose tissue mass and adipocyte size. Mechanistically, we showed that PSPC1 binds directly to a battery of adipose-specific mRNA transcripts via its 2 RRM domains. PSPC1 interacts with the RNA export factor DDX3X and translocates from the nucleus to the cytoplasm during the course of differentiation, thereby enhancing the nuclear export of its target transcripts. Loss of PSPC1 expression in adipose tissue in vivo compromises adipocyte development and lipid storage, and affects the development of diet-induced obesity and insulin resistance.

Previous work has linked a small number of RNA-binding proteins to adipocyte differentiation, most of which appear to be involved in RNA splicing. Alternatively spliced isoforms of the insulin receptor, lipin, nuclear receptor corepressor 1, and preadipocyte factor 1 (PREF-1) have all been associated with differentiation (49–52). More recently, the alternative-splicing factor SAM68 was found to regulate adipogenesis by modulating intron 5 retention in *mTOR* transcripts and isoform switching of ribosomal S6 kinase (18, 53). RNA-binding motif protein 4 (RBM4) has also been reported to regulate the splicing of adipocyte-specific genes, including the insulin receptor, PPARγ, and PREF-1, thereby facilitating brown adipocyte development (54). Whether other aspects of posttranscriptional RNA processing, such as mRNA export from the nucleus, mRNA turnover, and translation initiation, are also regulated during adipogenesis has heretofore been unclear (55–57). Furthermore, the importance of RNA processing factors for the development and function of adipose tissue in vivo has not been tested. Our data identify PSPC1-dependent maturation of adipocyte mRNAs as a new control point in the differentiation process.

In an effort to better understand how paraspeckle complexes may contribute to adipogenesis, we purified PSPC1-containing complexes. IP–mass spectrometry analysis identified a number of adipocyte-specific PSPC1 interaction partners, including DDX3X. These findings imply that in specific cellular contexts, the core paraspeckle components may recruit different proteins to the complex to accomplish tissue-specific functions. DDX3X belongs to the DEAD-box RNA helicase family, which has been implicated in many aspects of RNA metabolism, including transcription,

splicing, and export (41). Recent studies have highlighted the ability of DDX3X to shuttle between nucleus and cytoplasm and pointed to a role for DDX3X in RNA nuclear export (45–47). In the present study, we demonstrated that PSPC1 interacts with DDX3X in adipocytes but not in preadipocytes, and that this is associated with the maturation of a subset of adipocyte mRNAs. Knocking down DDX3X expression blunted the ability of PSPC1 to increase protein levels of its targets, strongly suggesting that DDX3X is an important effector of PSPC1's actions in adipogenesis.

Although DBHS proteins have been characterized as nuclear proteins, some evidence points to potential roles for them in the cytoplasm. For example, PSPC1, NONO, and SFPQ were isolated as part of an RNA-transporting granule in dendrites, suggesting a possible function in RNA transport in the cytoplasm. Interestingly, DDX3X was also purified from this granule, supporting our finding of DDX3X as an interaction partner of PSPC1 (58). Another study showed that NONO shuttles to the cytoplasm during cell fusion (59). We showed here that PSPC1 traffics from the nucleus to the cytoplasm during adipocyte differentiation. Moreover, translocation of PSPC1 to the cytoplasm was linked to the increased expression of a battery of adipose-specific proteins, including the key transcription factor EBF1. These results not only outline a new function for PSPC1, but also highlight an additional layer of regulatory complexity in the process of adipocyte development.

Reciprocal interactions exist between members of the DBHS protein family, and they have been found to form homo- and heterodimers in vivo (60). Their interaction raises the question of whether PSPC1 acts independently or in a complex with the other paraspeckle components in adipogenesis. PSPC1 indeed forms heterodimers with NONO and SFPQ during adipogenesis, with a stronger interaction observed in mature adipocytes than in preadipocytes. Furthermore, we observed translocation of NONO along with PSPC1 to the cytoplasm upon adipocyte differentiation, consistent with the possibility that paraspeckle proteins may function together in promoting mRNA maturation. However, ectopic expression of neither NONO nor SFPQ alone was able to facilitate adipocyte differentiation, suggesting either that PSPC1 may act independently of NONO and SFPQ, or that levels of PSPC1 may be limiting during differentiation. The question of whether PSPC1 acts in concert with NONO and SFPQ or with the noncoding RNA NEAT1 in adipocyte development remains to be addressed. Additional studies will also be required to dissect the precise molecular function(s) of PSPC1 in RNA maturation.

To assess how loss of PSPC1 in fat might affect metabolic health, we generated preadipocytes and mice lacking *Pspc1*. Consistent with our in vitro data, we observed impaired adipose tissue development in vivo when preadipocytes expressed a reduced amount of PSPC1. Adipose PSPC1–deficient mice did not present with lipodystrophy on normal chow diet, indicating that PSPC1 function is not absolutely required for adipose tissue lipid storage. However, the mice were markedly resistant to high-fat diet–induced obesity, with diminished mass of both subcutaneous and visceral WAT. Histology revealed reduced adipocyte size, similar to that observed in heterozygous PPARγ-deficient mice (61). Furthermore, despite their apparent reduced adipose tissue lipid storage capacity, adipose PSPC1–deficient mice did not show expected systemic consequences of profound lipodystrophy; rather, loss

of adipose PSPC1 in a high-fat diet–fed state resulted in improved glucose tolerance and insulin sensitivity.

Previous studies have found that impairment of mature adipocyte function, including alterations in lipogenesis and lipolysis, can provoke compensatory responses in other metabolic tissues (62, 63). For example, such compensatory effects have been observed with *Pparg* hypomorphic mice. Despite being lipodystrophic, these mice exhibit relatively benign metabolic consequences due to induction of a gene expression program in muscle that enables efficient oxidation of excess lipids (64). A second adipose-specific *aP2-Cre*–driven *Pparg* knockout model also demonstrated improved glucose tolerance on high-fat diet, possibly due to a compensatory increase in hepatic glucose disposal (65). Consistent with these findings, we observed that loss of PSPC1 expression in fat led to an increase in genes linked to thermogenesis in BAT and fatty acid utilization in skeletal muscle. Increased expression of skeletal muscle GLUT4 further suggests that enhanced muscle glucose uptake is likely to contribute to improved glucose tolerance and insulin sensitivity.

Methods

Reagents and plasmids. Dexamethasone (D2915), 3-isobutyl-1-methylxanthine (IBMX, I7018), PPARγ agonist GW1929 (G5668), and actinomycin D (A1410) were from Sigma-Aldrich. Insulin (12585-014) was from Gibco. PSPC1 shRNA sequences were designed using BLOCK-iT RNAi designer tool (Invitrogen). Sense and antisense oligos were annealed and cloned into pENTR/U6 plasmid (Invitrogen). Using LR recombination (Invitrogen), shRNA constructs were subcloned into a Gateway-adapted pBabe-Puro plasmid. The following shRNA oligos were used: lacZ shRNA, CACCGGGCCAGCTG-TATAGACATCTCGAAAGATGTCTATACAGCTGGCCC; PSPC1 shRNA1, CACCGGTTGTTTCCAATGAGCTTCTCGAAAGAAGCT-CATTGGAAACAACC; PSPC1 shRNA2, CACCGCGGCTTTAAAC-CAAACTATACGAATATAGTTTGGTTTAAAGCCGC; and PSPC1 shRNA3, CACCGCAAATATGGGAACTCCAATGCGAACATTG-GAGTTCCCATATTTGC. Only sense strands are shown here. ON-TARGETplus mouse DDX3X siRNA SMARTpool (L-043597) and Non-targeting Pool (D-001810) were from Dharmacon. Adenovirus was amplified, purified, and titered by Viraquest Inc.

Cell culture. 3T3-L1, 3T3-F442A, and NIH-3T3 cells were obtained from ATCC and cultured in DMEM supplemented with 10% bovine calf serum. 10T1/2 preadipocytes and murine brown preadipocytes were cultured in DMEM with 10% FBS. For white adipocyte differentiation, preadipocytes were grown to confluence in DMEM with 10% FBS plus insulin (5 μg/ml). Confluent cells were induced to differentiate with dexamethasone (1 μM), IBMX (0.5 mM), insulin (5 μg/ml), and GW1929 for 2 days, followed by insulin and GW1929 alone. For brown adipocyte differentiation, cells were plated in DMEM containing 10% FBS plus insulin (5 μg/ml) and T3 (1 nM). After confluence, cells were stimulated to differentiate with dexamethasone (5 μM), IBMX (0.5 mM), indomethacin (125 μM), insulin (5 μg/ml), T3 (1 nM), and GW1929 for 2 days, followed by insulin (5 μg/ml), T3 (1 nM), and GW1929. Growth medium was exchanged every 2 days during the course of differentiation. Brown preadipocytes were isolated and immortalized as described (66). All stable cells were generated using the pBabe retroviral system (67). Preadipocytes were transduced with retrovirus overnight and selected with particular antibiotics. For RNA

stability studies, differentiated adipocytes were treated with actinomycin D (4 μg/ml). RNA samples were collected before and at multiple time points after the treatment.

Gene expression analysis. Total RNA was isolated using TRIzol reagent (Invitrogen) and reverse transcribed with the iScript cDNA synthesis kit (Bio-Rad). cDNA was quantified by real-time PCR using SYBR Green Master Mix (Diagenode) on an ABI 7900 instrument. Gene expression levels were determined using a standard curve. Each gene was normalized to the housekeeping gene *36B4* and was analyzed in duplicate. Primers used for real-time PCR are listed in Supplemental Table 4.

Protein analysis. Whole cell lysate was extracted using RIPA lysis buffer (Boston Bioproducts) supplemented with complete protease inhibitor cocktail (Roche). Proteins were diluted in NuPAGE loading dye (Invitrogen), heated at 95°C for 5 minutes, and run on 4%–12% NuPAGE Bis-Tris Gel (Invitrogen). Proteins were transferred to Hybond ECL membrane (GE Healthcare) and blotted with PSPC1 (ab115184, Abcam), PPARγ (81B8, Cell Signaling), EBF1 (ab108369, Abcam), SCD1 (sc14719, Santa Cruz Biotechnology), ACSL1 (4047S, Cell Signaling), NONO (N8789, Sigma-Aldrich), DDX3X (ab37160, Abcam), PPM1B (A300-887A, Bethyl Labs), V5 (R960-25, Invitrogen), HMG1 (ab18256, Abcam), actin (A2066, Sigma-Aldrich), and α-tubulin (CP06, Calbiochem) antibodies. Band intensities of scanned blots were quantified using ImageJ computer software (NIH).

Chromatin immunoprecipitation. ChIP assays were performed according to a standard protocol (30). Briefly, following formaldehyde cross-linking, cells were lysed and sonicated using Bioruptor (Diagenode) according to the manufacturer's protocol. Chromatin was immunoprecipitated with antibodies against PPARγ (sc7196, Santa Cruz Biotechnology) and RXR (sc774, Santa Cruz Biotechnology) overnight at 4°C in the presence of Protein A/G PLUS agarose beads (Santa Cruz Biotechnology). After reversal of cross-linking, DNA was extracted and DNA enrichment was quantified by real-time PCR. Primers used were: *Pspc1* –0.2 kb forward, TGGAGGAGGGGGTTGTTTG; *Pspc1* –0.2 kb reverse, CCGGAGGGTCGAAAGCTAAG; *Hbb* (hemoglobin beta) forward, TGGTAGCCTCAGGAGCTTGC; *Hbb* reverse, ATCCAAGATGGGACCAAGCTG. Occupancy was quantified using a standard curve and normalized to input DNA.

iCLIP and sequencing. iCLIP assays were performed according to a modified protocol (37, 68). Briefly, 10T1/2 cells expressing Flag-PSPC1 were irradiated with 254 nm UV-C light at 800 mJ/cm² on ice to cross-link proteins to nucleic acids. Upon cell lysis, protein-RNA complexes were immunoprecipitated with anti-Flag M2 antibody (F1804, Sigma-Aldrich) immobilized on Dynabeads Protein G (10003D, Novex) overnight. After high-salt stringent washing, RNAs on beads were partially fragmented using micrococcal nuclease (M0247S, New England Biolabs), ligated to an RNA adaptor at the 3′ end, and radioactively labeled on the 5′ end. Protein-RNA complexes were eluted using 3X Flag peptides (F4799, Sigma-Aldrich) and run on 4%–12% NuPAGE Bis-Tris Gel (Invitrogen). After transfer to nitrocellulose membranes, protein-RNA complexes in the range of 20–40 kDa above Flag-PSPC1 were recovered and digested with proteinase K. Reverse transcription was done with SuperScript III Reverse Transcriptase (18080044, Invitrogen), using primers containing 2 inversely oriented adaptor regions separated by a *Bam*HI site as well as a 3-nt barcode to mark individual cDNA molecules. cDNAs were size-purified using denaturing gel electrophoresis, circularized by CircLigase II ssDNA ligase (CL9021K, Epicentre), and linearized by FastDi-

gest *Bam*HI (FD0054, Thermo Fisher Scientific). Linearized cDNAs were PCR-amplified and subjected to high-throughput sequencing (single end 100 nt) using Illumina HiSeq2000.

iCLIP-Seq data analysis. CLIP-Seq reads were trimmed to remove adaptor sequences and categorized according to different barcodes. To eliminate redundancies created by PCR duplicates, all reads with identical adaptor sequence were considered a single read. Quality control check was applied to all the trimmed reads using the FastQC tool from Babraham Bioinformatics. CLIP-Seq reads of at least 12 nt in length were mapped to the mouse genome (NCBI37/mm9) using the TopHat alignment pipeline on UCLA Galaxy platform with parameters set to search for unique alignment, with fewer than 2 mismatches, and with no indels. Mapped reads were then subjected to the CLIP-Seq cluster-finding algorithm CLIPper to call significant (FDR < 0.05, $P < 0.05$) clusters (39). Significant clusters were uploaded onto the University of California, Santa Cruz, Genome Browser as custom annotation tracks. Read distribution over the genome was analyzed using the RSeQC tool (69). De novo motif search was performed using the HOMER findMotifsGenome program with parameters -rna -S 10 -len 4,5,6 -size given -h -nlen 0 -noweight. Background sequences were from CLIP-Seq reads of the experimental control library (40).

Co-IP and mass spectrometry. Cells expressing Flag-PSPC1 were lysed with ice-cold lysis buffer containing 50 mM Tris-HCl pH 7.5, 150 mM NaCl, 0.6% Triton X-100, plus complete protease inhibitor (Roche). Cell lysates were precleared with empty Protein A/G PLUS agarose beads (Santa Cruz Biotechnology) and then immunoprecipitated with beads prelinked with anti-Flag M2 antibody (F1804, Sigma-Aldrich) overnight at 4°C. Beads were washed with 50 mM Tris-HCl pH 7.5, 150 mM NaCl, and 0.1% Triton X-100, then eluted with 3X Flag peptides (F4799, Sigma-Aldrich). In specific experiments, RNase (AM2286, Ambion) was used to treat cell lysates before IP. IP eluents from Flag-PSPC1 cells and control cells were processed by nano–liquid chromatography with data-dependent tandem mass spectrometry performed on an Orbitrap mass spectrometer (70). The results were analyzed using Mascot software (Matrix Sciences).

Subcellular fractionation. Cells were washed with 1× PBS and incubated with TEN buffer (10 mM Tris-HCl pH 7.5, 100 mM NaCl, 1 mM EDTA pH 8.0). Cells were allowed to swell on ice for 15 minutes in 10 mM HEPES, 10 mM KCl, 0.1 mM EGTA, 0.1 mM EDTA, 1 mM DTT, plus complete protease inhibitor (Roche). Cells were then mixed with NP-40 alternative (Calbiochem) to a final concentration of 0.4%, incubated for 5 minutes, and centrifuged at 12,000 *g* for 5 minutes. Supernatant was collected as the cytoplasmic fraction. Nuclear pellet was resuspended in 20 mM HEPES, 420 mM NaCl, 1.5 mM MgCl$_2$, 0.2 mM EDTA, 25% glycerol, 1 mM DTT, plus complete protease inhibitor. After a 15-minute incubation, nuclear extracts were spun at 12,000 *g* for 5 minutes, and the supernatant was saved for future analysis. For RNA analysis, all the buffers above were supplemented with 10 mM ribonucleoside-vanadyl complex (New England Biolabs) to inhibit ribonucleases. RNA was extracted from the nuclear and cytoplasmic fraction using a Purelink kit (Ambion).

Immunofluorescence. 10T1/2 cells were plated in gelatin-coated glass-bottom dishes (MatTek). At day 0 and day 6 of differentiation, cells were fixed with 4% paraformaldehyde in PBS. Cells were permeabilized with 0.1% Triton and treated with NH$_4$Cl to quench free aldehyde groups. Cells were then blocked with 5% normal goat serum (Vector Laboratories) and 1% BSA (Sigma-Aldrich) in PBS for 30 minutes. Cells were incubated with V5 (R960-25, Invitrogen) or Psps1 (sc374181, Santa Cruz Biotechnology) antibody in blocking buffer overnight at 4°C. After washes, cells were incubated with Alexa Fluor 594–conjugated secondary antibody (A-21125, Invitrogen) for 1 hour at room temperature and washed. Cells were stained with BODIPY 493/503 (Invitrogen) and/or DAPI (Invitrogen). Cells were visualized with an LSM510 confocal laser scanning microscope (Carl Zeiss).

Pspc1 adipose-specific knockout mice. A conditional-potential knockout allele for *Pspc1* was generated using a "targeted trapping/conditional-ready" gene-targeting vector (*Pspc1*^tm1a) (Supplemental Figure 8B). The targeting vector was electroporated into C57BL/6N ES cell line JM8.N4. Out of 12 validated targeted ES cell clones, a euploid clone (clone A11) was selected for in vitro Flp recombination. Flp recombinase excised the gene-trapping cassette within intron 1 of *Pspc1*, producing a conditional knockout allele containing a *loxP* site in intron 1 and a *loxP* site in intron 2. Genotyping was completed by amplification of the genomic region flanking loxP sites using the following primer pairs: forward ACGTAGCCCAGGTAGGTATTTCAGG and reverse TGTAACAAGATCTGATGTCCTCTTCTGG (Supplemental Figure 8C). Eleven clones passed Flp testing, and clone A11_flp_A09 was selected and injected into BALB/c blastocysts to generate chimeric mice. High-percentage male chimeras were obtained, and were crossed to C57BL/6N mice to establish germline transmission. Homozygous *Pspc1*-floxed mice were crossed with adiponectin-*Cre* mice (a gift of Evan Rosen, Beth Israel Hospital, Boston, Massachusetts, USA) to generate adipose-specific PSPC1-deficient mice.

Animal studies. For the preadipocyte transplantation study, 6-week-old male NCr nude mice were acquired from Taconic. Mice were anesthetized using 2%–3% isoflurane in O$_2$. Using an insulin syringe attached to a 28-gauge needle, 2×10^7 3T3-F442A preadipocytes were injected subcutaneously over the sternum. Newly formed subcutaneous fat pads were dissected, weighed, and processed for histological and gene expression analysis. Homozygous *Pspc1*-floxed mice carrying the conditional-ready knockout allele were used for adenovirus-Cre injection studies. For the adenovirus delivery to fat pads, 2×10^9 PFU of adenovirus was percutaneously injected into the inguinal fat depot at 8 weeks of age (71). In each mouse, Ad-Cre was injected on one side, and Ad-GFP was injected on the contralateral side. Seven days after the injection, iWAT was resected for analysis. At 10 weeks of age, *Pspc1*^fl/fl *Cre*+ mice and their *Pspc1*^fl/fl littermates were fed a 60% high-fat diet (Research Diets) for the indicated times. For glucose tolerance tests, mice were fasted for 6 hours and challenged with an i.p. injection of glucose (2 g/kg). For insulin tolerance tests, mice were fasted for 6 hours and given an i.p. injection of insulin (1 U/kg). Blood glucose levels were monitored using the Accu-Chek active glucometer (Roche). Body composition was determined by EchoMRI analysis. Indirect calorimetry was performed using a Columbus Instruments Comprehensive Lab Animal Monitoring System. Animals were placed individually in chambers for 3 consecutive days at ambient temperature (26.5°C) with 12-hour light/dark cycles. Respiratory measurements were made in 20-minute intervals after an initial 7- to 9-hour acclimation period. Energy expenditure rate (EE) was calculated from VO$_2$ and respiratory exchange ratio (RER) using the Lusk equation, EE in kcal/kg/h = $(3.815 + 1.232 \times \text{RER}) \times$ VO$_2$ in ml/kg/h. Statistical significance for EE, VO$_2$, and VCO$_2$ measurements was determined by 2-way ANOVA. Analysis of EE with body mass or lean mass as covari-

ate was assessed via ANCOVA using the National Mouse Metabolic Phenotyping Centers ANCOVA data analysis tool (http://mmpc.org/). Serum triglyceride and cholesterol were measured using a Wako Diagnostics L-Type TG M test and Cholesterol E test.

Statistics. All data are presented as mean + SEM and were analyzed using Prism (GraphPad) computer software. Unpaired 2-tailed Student's *t* test was used for single-variable comparison between 2 groups. One-way ANOVA followed by Dunnett post hoc test was used for multiple comparisons versus the control group. Two-way ANOVA followed by Bonferroni post-tests was used to examine interactions between multiple variables. P less than 0.05 was considered to be statistically significant and is presented as $^*P < 0.05$ or $^{**}P < 0.01$.

Study approval. Animal experiments were approved by the UCLA Institutional Animal Care and Research Advisory Committee.

1. Rosen ED, MacDougald OA. Adipocyte differentiation from the inside out. *Nat Rev Mol Cell Biol*. 2006;7(12):885–896.

2. Tontonoz P, Hu E, Graves RA, Budavari AI, Spiegelman BM. mPPARγ 2: tissue-specific regulator of an adipocyte enhancer. *Genes Dev*. 1994;8(10):1224–1234.

3. Tontonoz P, Hu E, Spiegelman BM. Stimulation of adipogenesis in fibroblasts by PPARγ 2, a lipid-activated transcription factor. *Cell*. 1994;79(7):1147–1156.

4. Tontonoz P, Hu E, Devine J, Beale EG, Spiegelman BM. PPARγ 2 regulates adipose expression of the phosphoenolpyruvate carboxykinase gene. *Mol Cell Biol*. 1995;15(1):351–357.

5. Schoonjans K, et al. PPARα and PPARγ activators direct a distinct tissue-specific transcriptional response via a PPRE in the lipoprotein lipase gene. *EMBO J*. 1996;15(19):5336–5348.

6. Dalen KT, et al. Adipose tissue expression of the lipid droplet-associating proteins S3-12 and perilipin is controlled by peroxisome proliferator-activated receptor-γ. *Diabetes*. 2004;53(5):1243–1252.

7. Yeh WC, Cao Z, Classon M, McKnight SL. Cascade regulation of terminal adipocyte differentiation by three members of the C/EBP family of leucine zipper proteins. *Genes Dev*. 1995;9(2):168–181.

8. Oishi Y, et al. Krüppel-like transcription factor KLF5 is a key regulator of adipocyte differentiation. *Cell Metab*. 2005;1(1):27–39.

9. Jimenez MA, Akerblad P, Sigvardsson M, Rosen ED. Critical role for Ebf1 and Ebf2 in the adipogenic transcriptional cascade. *Mol Cell Biol*. 2007;27(2):743–757.

10. Smas CM, Sul HS. Pref-1, a protein containing EGF-like repeats, inhibits adipocyte differentiation. *Cell*. 1993;73(4):725–734.

11. Tong Q, Dalgin G, Xu H, Ting CN, Leiden JM, Hotamisligil GS. Function of GATA transcription factors in preadipocyte-adipocyte transition. *Science*. 2000;290(5489):134–138.

12. Ross SE, et al. Inhibition of adipogenesis by Wnt signaling. *Science*. 2000;289(5481):950–953.

13. Puigserver P, Wu Z, Park CW, Graves R, Wright M, Spiegelman BM. A cold-inducible coactivator of nuclear receptors linked to adaptive thermogenesis. *Cell*. 1998;92(6):829–839.

14. Villanueva CJ, et al. TLE3 is a dual-function transcriptional coregulator of adipogenesis. *Cell Metab*. 2011;13(4):413–427.

15. Seale P, et al. PRDM16 controls a brown fat/skeletal muscle switch. *Nature*. 2008;454(7207):961–967.

16. Kim SY, et al. miR-27a is a negative regulator of adipocyte differentiation via suppressing PPARγ expression. *Biochem Biophys Res Commun*. 2010;392(3):323–328.

17. Sun T, Fu M, Bookout AL, Kliewer SA, Mangelsdorf DJ. MicroRNA let-7 regulates 3T3-L1 adipogenesis. *Mol Endocrinol*. 2009;23(6):925–931.

18. Huot MÉ, et al. The Sam68 STAR RNA-binding protein regulates mTOR alternative splicing during adipogenesis. *Mol Cell*. 2012;46(2):187–199.

19. Zhao XY, Li S, Wang GX, Yu Q, Lin JD. A long noncoding RNA transcriptional regulatory circuit drives thermogenic adipocyte differentiation. *Mol Cell*. 2014;55(3):372–382.

20. Fox AH, et al. Paraspeckles: a novel nuclear domain. *Curr Biol*. 2002;12(1):13–25.

21. Patton JG, Porro EB, Galceran J, Tempst P, Nadal-Ginard B. Cloning and characterization of PSF, a novel pre-mRNA splicing factor. *Genes Dev*. 1993;7(3):393–406.

22. Yang YS, Hanke JH, Carayannopoulos L, Craft CM, Capra JD, Tucker PW. NonO, a non-POU-domain-containing, octamer-binding protein, is the mammalian homolog of Drosophila nonAdiss. *Mol Cell Biol*. 1993;13(9):5593–5603.

23. Peng R, Dye BT, Pérez I, Barnard DC, Thompson AB, Patton JG. PSF and p54nrb bind a conserved stem in U5 snRNA. *RNA*. 2002;8(10):1334–1347.

24. Kaneko S, Rozenblatt-Rosen O, Meyerson M, Manley JL. The multifunctional protein p54nrb/PSF recruits the exonuclease XRN2 to facilitate pre-mRNA 3′ processing and transcription termination. *Genes Dev*. 2007;21(14):1779–1789.

25. Kameoka S, Duque P, Konarska MM. p54(nrb) associates with the 5′ splice site within large transcription/splicing complexes. *EMBO J*. 2004;23(8):1782–1791.

26. Kuwahara S, et al. PSPC1, NONO, and SFPQ are expressed in mouse Sertoli cells and may function as coregulators of androgen receptor-mediated transcription. *Biol Reprod*. 2006;75(3):352–359.

27. Myojin R, et al. Expression and functional significance of mouse paraspeckle protein 1 on spermatogenesis. *Biol Reprod*. 2004;71(3):926–932.

28. Waki H, et al. The small molecule harmine is an antidiabetic cell-type-specific regulator of PPARγ expression. *Cell Metab*. 2007;5(5):357–370.

29. Villanueva CJ, et al. Adipose subtype-selective recruitment of TLE3 or Prdm16 by PPARγ specifies lipid storage versus thermogenic gene programs. *Cell Metab*. 2013;17(3):423–435.

30. Nielsen R, et al. Genome-wide profiling of PPARgamma:RXR and RNA polymerase II occupancy reveals temporal activation of distinct metabolic pathways and changes in RXR dimer composition during adipogenesis. *Genes Dev*. 2008;22(21):2953–2967.

31. Fox AH, Bond CS, Lamond AI. P54nrb forms a heterodimer with PSP1 that localizes to paraspeckles in an RNA-dependent manner. *Mol Biol Cell*. 2005;16(11):5304–5315.

32. Gernapudi R, et al. MicroRNA 140 promotes expression of long noncoding RNA NEAT1 in adipogenesis. *Mol Cell Biol*. 2016;36(1):30–38.

33. Bond CS, Fox AH. Paraspeckles: nuclear bodies built on long noncoding RNA. *J Cell Biol*. 2009;186(5):637–644.

34. Maris C, Dominguez C, Allain FH. The RNA recognition motif, a plastic RNA-binding platform to regulate post-transcriptional gene expression. *FEBS J*. 2005;272(9):2118–2131.

35. Bandziulis RJ, Swanson MS, Dreyfuss G. RNA-binding proteins as developmental regulators. *Genes Dev*. 1989;3(4):431–437.

36. Konig J, et al. iCLIP — transcriptome-wide mapping of protein-rna interactions with individual nucleotide resolution. *J Vis Exp*. 2011;(50):e2638.

37. Damianov A, et al. Rbfox proteins regulate splicing as part of a large multiprotein complex LASR. *Cell*. 2016;165(3):606–619.

38. Trapnell C, Pachter L, Salzberg SL. TopHat: discovering splice junctions with RNA-Seq. *Bioinformatics*. 2009;25(9):1105–1111.

39. Lovci MT, et al. Rbfox proteins regulate alternative mRNA splicing through evolutionarily conserved RNA bridges. *Nat Struct Mol Biol*. 2013;20(12):1434–1442.

40. Heinz S, et al. Simple combinations of lineage-determining transcription factors prime cis-regulatory elements required for macrophage and B cell identities. *Mol Cell*. 2010;38(4):576–589.

41. Rocak S, Linder P. DEAD-box proteins: the driv-

ing forces behind RNA metabolism. *Nat Rev Mol Cell Biol*. 2004;5(3):232–241.

42. Jarmoskaite I, Russell R. RNA helicase proteins as chaperones and remodelers. *Annu Rev Biochem*. 2014;83:697–725.

43. Sharma D, Jankowsky E. The Ded1/DDX3 subfamily of DEAD-box RNA helicases. *Crit Rev Biochem Mol Biol*. 2014;49(4):343–360.

44. Soto-Rifo R, Ohlmann T. The role of the DEAD-box DDX3 in mRNA metabolism. *Wiley Interdiscip Rev RNA*. 2013;4(4):369–385.

45. Lai MC, Lee YH, Tarn WY. The DEAD-box RNA helicase DDX3 associates with export messenger ribonucleoproteins as well as tip-associated protein and participates in translational control. *Mol Biol Cell*. 2008;19(9):3847–3858.

46. Yedavalli VS, Neuveut C, Chi YH, Kleiman L, Jeang KT. Requirement of DDX3 DEAD box RNA helicase for HIV-1 Rev-RRE export function. *Cell*. 2004;119(3):381–392.

47. Sharma D, Bhattacharya J. Evolutionary constraints acting on DDX3X protein potentially interferes with Rev-mediated nuclear export of HIV-1 RNA. *PLoS One*. 2010;5(3):e9613.

48. Tran TT, Kahn CR. Transplantation of adipose tissue and stem cells: role in metabolism and disease. *Nat Rev Endocrinol*. 2010;6(4):195–213.

49. Entingh AJ, Taniguchi CM, Kahn CR. Bidirectional regulation of brown fat adipogenesis by the insulin receptor. *J Biol Chem*. 2003;278(35):33377–33383.

50. Péterfy M, Phan J, Reue K. Alternatively spliced lipin isoforms exhibit distinct expression pattern, subcellular localization, and role in adipogenesis. *J Biol Chem*. 2005;280(38):32883–32889.

51. Goodson ML, Mengeling BJ, Jonas BA, Privalsky ML. Alternative mRNA splicing of corepressors generates variants that play opposing roles in adipocyte differentiation. *J Biol Chem*. 2011;286(52):44988–44999.

52. Mei B, Zhao L, Chen L, Sul HS. Only the large soluble form of preadipocyte factor-1 (Pref-1), but not the small soluble and membrane forms, inhibits adipocyte differentiation: role of alternative splicing. *Biochem J*. 2002;364(pt 1):137–144.

53. Song J, Richard S. Sam68 Regulates S6K1 Alternative Splicing during Adipogenesis. *Mol Cell Biol*. 2015;35(11):1926–1939.

54. Lin JC, Tarn WY, Hsieh WK. Emerging role for RNA binding motif protein 4 in the development of brown adipocytes. *Biochim Biophys Acta*. 2014;1843(4):769–779.

55. Hu YJ, et al. Transcriptional and post-transcriptional control of adipocyte differentiation by Jumonji domain-containing protein 6. *Nucleic Acids Res*. 2015;43(16):7790–7804.

56. Yu H, et al. Stk40 represses adipogenesis through translational control of CCAAT/enhancer-binding proteins. *J Cell Sci*. 2015;128(15):2881–2890.

57. Cho H, et al. Staufen1-mediated mRNA decay functions in adipogenesis. *Mol Cell*. 2012;46(4):495–506.

58. Kanai Y, Dohmae N, Hirokawa N. Kinesin transports RNA: isolation and characterization of an RNA-transporting granule. *Neuron*. 2004;43(4):513–525.

59. Zolotukhin AS, et al. PSF acts through the human immunodeficiency virus type 1 mRNA instability elements to regulate virus expression. *Mol Cell Biol*. 2003;23(18):6618–6630.

60. Fox AH, Lamond AI. Paraspeckles. *Cold Spring Harb Perspect Biol*. 2010;2(7):a000687.

61. Kubota N, et al. PPARγ mediates high-fat diet-induced adipocyte hypertrophy and insulin resistance. *Mol Cell*. 1999;4(4):597–609.

62. Lodhi IJ, et al. Inhibiting adipose tissue lipogenesis reprograms thermogenesis and PPARγ activation to decrease diet-induced obesity. *Cell Metab*. 2012;16(2):189–201.

63. Polak P, Cybulski N, Feige JN, Auwerx J, Rüegg MA, Hall MN. Adipose-specific knockout of raptor results in lean mice with enhanced mitochondrial respiration. *Cell Metab*. 2008;8(5):399–410.

64. Koutnikova H, et al. Compensation by the muscle limits the metabolic consequences of lipodystrophy in PPARγ hypomorphic mice. *Proc Natl Acad Sci U S A*. 2003;100(24):14457–14462.

65. Jones JR, et al. Deletion of PPARgamma in adipose tissues of mice protects against high fat diet-induced obesity and insulin resistance. *Proc Natl Acad Sci U S A*. 2005;102(17):6207–6212.

66. Villanueva CJ, et al. Adipose subtype-selective recruitment of TLE3 or Prdm16 by PPARγ specifies lipid storage versus thermogenic gene programs. *Cell Metab*. 2013;17(3):423–435.

67. Hummasti S, Tontonoz P. The peroxisome proliferator-activated receptor N-terminal domain controls isotype-selective gene expression and adipogenesis. *Mol Endocrinol*. 2006;20(6):1261–1275.

68. König J, et al. iCLIP reveals the function of hnRNP particles in splicing at individual nucleotide resolution. *Nat Struct Mol Biol*. 2010;17(7):909–915.

69. Wang L, Wang S, Li W. RSeQC: quality control of RNA-seq experiments. *Bioinformatics*. 2012;28(16):2184–2185.

70. Patananan AN, Capri J, Whitelegge JP, Clarke SG. Non-repair pathways for minimizing protein isoaspartyl damage in the yeast Saccharomyces cerevisiae. *J Biol Chem*. 2014;289(24):16936–16953.

71. Ma X, et al. Celastrol protects against obesity and metabolic dysfunction through activation of a HSF1-PGC1α transcriptional axis. *Cell Metab*. 2015;22(4):695–708.